Latrophilin-2 repels Teneurin-3+ hippocampal axons during target selection

Daniel T. Pederick[1], Jan H. Lui[1], Ellen C. Gingrich[1,2], Chuanyun Xu[1] , Yuanyuan Liu[3,6], Zhigang He[3], Stephen R. Quake[4,5], Liqun Luo[1, *]

[1]Department of Biology, Howard Hughes Medical Institute, Stanford University, USA
[2]Neurosciences Graduate Program, Stanford University, USA
[3]F.M. Kirby Neurobiology Center, Department of Neurology, Boston Children's Hospital, Harvard Medical School, Boston, MA 02115, USA
[4]Departments of Bioengineering and Applied Physics, Stanford University, USA
[5]Chan Zuckerberg Biohub, Stanford, CA 94305, USA
[6]Current address: Somatosensation and Pain Unit, National Institute of Dental and Craniofacial Research (NIDCR), National Center for Complementary and Integrative Health (NCCIH), National Institutes of Health, Bethesda MD 20892

*Corresponding author (email: lluo@stanford.edu)

Spatial- and object-related signals are preferentially processed through the medial and lateral hippocampal networks (MHN and LHN), respectively[1,2]. MHN comprises interconnected medial entorhinal cortex, proximal CA1 (pCA1), and distal subiculum (dSub), whereas the LHN comprises interconnected lateral entorhinal cortex, distal CA1, and proximal subiculum[3,4]. Previously, we showed that Teneurin-3 (Ten3) has matching expression in all interconnected regions of the MHN and is required in both CA1 and subiculum for the precise pCA1→dSub axon targeting through homophilic attraction[5]. Can matching gene expression in interconnected nodes of the LHN also contribute to hippocampal network assembly? Here, we discovered that latrophilin-2 (Lphn2), an adhesion GPCR known to bind teneurins[6–8], has matching expression in the LHN that is complementary to Ten3. Viral-genetic perturbations *in vivo* revealed that Ten3+ pCA1 axons are repelled by ectopic expression of Lphn2 in dSub, and ectopically invade proximal subiculum deleted for *Lphn2*. Simultaneous subiculum deletion of *Lphn2* and *Ten3* causes Ten3+ pCA1 axon mistargeting reflecting loss of both repulsion and attraction. Our findings demonstrate that Lphn2 acts as a repulsive ligand for Ten3+ axons, identify Ten3 as a receptor for both repulsive and attractive ligands in the same axon during target choice, and reveal how a 'Ten3→Ten3, Lphn2→Lphn2' rule directs the precise assembly of functional hippocampal networks.

In order for the central nervous system to accurately process information, neurons must connect precisely with their correct targets. Neuronal circuit assembly can generally be divided into three steps: 1) axons are guided to the appropriate anatomical region; 2) axons select specific target neurons within the region; and 3) axons form synapses with target neurons[9]. Molecular mechanisms underlying axon guidance and synapse formation/organization have been revealed over the last several decades[10–12]. Less is known about the mechanisms of target selection, particularly in complex circuits of the central mammalian brain. The differential expression of cell surface molecules plays a critical role in allowing discrete neuronal circuits to be formed precisely[9,13]. For example, a pair of evolutionarily conserved type II transmembrane proteins,

Teneurins, instruct synaptic partner selection in the *Drosophila* olfactory and neuromuscular circuits via matching expression in synaptic partners and homophilic attraction[14,15]. Mammals have four Teneurins (*Ten1–4*), which are differentially expressed in the developing nervous system[16] and play roles in cortical cell migration[17], visual and thalamostriatal systems wiring[18–21], and synapse formation[22]. Mutations in human Teneurins are implicated in various nervous system disorders including bipolar disorder[23–25], schizophrenia[26], microphthalmia[27] and congenital general anosmia[28].

We have previously shown that mouse Ten3 has matching expression in interconnected areas of the hippocampal network[5]. The hippocampus has topographically organized projections along the proximal-distal axis. Specifically, proximal CA1 (pCA1) projects axons to distal subiculum (dSub), and distal CA1 (dCA1) projects axons to proximal subiculum (pSub). Both pCA1 and dSub also form reciprocal connections with the medial entorhinal cortex (MEC), forming the medial hippocampal network (MHN), whereas both dCA1 and pSub form reciprocal connections with the lateral entorhinal cortex (LEC), forming the lateral hippocampal network (LHN)[3,4] (**Fig. 1a**). Ten3 is highly expressed in pCA1, dSub, and MEC (**Extended Data Fig. 1a**), is required in both pCA1 and dSub for the precise target selection of the pCA1→dSub axons, and acts as a homophilic adhesion molecule[5]. These data support a homophilic attraction mechanism for Ten3 in regulating the pCA1→dSub axon projection. However, it remains unclear if matching gene expression in the LHN exists and, if so, how this contributes to precise hippocampal network formation.

Genes with inverse expression to Ten3

We hypothesized that cell surface molecules that are specifically expressed in the LHN and thus have c omplementary expression to Ten3 may play a role in the precise assembly of the hippocampal network. To identify such genes, we performed fluorescence-activated cell sorting-based single-cell RNA sequencing (scRNA-seq) of postnatal day (P) 8 excitatory neurons, in medial network subregions (pCA1, dSub, and MEC) or lateral network subregions (dCA1, pSub, and LEC) (**Extended Data Fig. 1a**). We chose P8 to coincide with the period of target selection for pCA1→dSub axons[5]. Single cells from contaminating adjacent regions were removed from the dataset or relabeled based on the expression of known marker genes (**Extended Data Fig. 2**). Representation of the scRNA-seq data in the tSNE space (**Extended Data Fig. 1b**) revealed clusters that segregated partially by subregions, but did not clearly delineate the lateral versus medial hippocampal networks. Instead, every cluster contained a combination of cells predominantly from one of the larger regions (CA1, subiculum, and entorhinal cortex), and *Ten3*-expressing cells were generally present across all regions/clusters (**Extended Data Fig. 1c**). We therefore used the 'ground-truth' that Ten3 has enriched expression in all medial network regions and is functionally important for MHN assembly[5] to specifically search for genes with complementary expression patterns to *Ten3* in each of the regions.

We compared the gene expression of cells highly expressing *Ten3* (>95th percentile, *Ten3*-HIGH) with those that did not express *Ten3* (*Ten3*-NONE) within each large region (CA1, subiculum, or entorhinal cortex), tabulating genes with higher average expression in the *Ten3*-NONE group for each region. By computing the intersection of these lists, we found only eleven genes, of which only three

corresponded to putative cell surface molecules (**Fig. 1b**; **Extended Data Fig. 1d-f**). Interestingly, *Lphn2*, an adhesion G-protein-coupled receptor (GPCR) known to bind Teneurins[6–8,17,22,29], was one of the three cell surface molecules that showed inverse expression to *Ten3* in CA1, subiculum, and entorhinal cortex (**Fig. 1c**). Teneurins interact in *trans* with Latrophilins, and this interaction has been implicated in multiple neurodevelopmental processes[17,22,30]. This finding suggests that Lphn2 may participate in hippocampal network assembly.

Inverse expression of Lphn2 and Ten3

To validate the finding from our scRNA-seq screen, we performed *in situ* expression analysis on P8 brains. Double *in situ* hybridization for *Lphn2* mRNA and *Ten3* mRNA revealed specific expression of *Lphn2* in dCA1, pSub, and LEC, which was strikingly complementary to *Ten3* enrichment in pCA1, dSub, and MEC (**Fig. 1d, Extended Data Fig. 3a**). Quantification of *Lphn2* and *Ten3* mRNA showed opposing gradients of expression, with *Lphn2* expression levels increasing more sharply after the *Ten3*-high zone in CA1 and subiculum compared to entorhinal cortex (**Fig. 1e, Extended Data Fig. 3b**). We also examined protein expression by using an anti-Ten3 antibody[5] and an anti-GFP antibody in *Lphn2-Venus*-knockin mice[31]. In all regions, Lphn2 and Ten3 proteins were inversely expressed in the synaptic layers corresponding to their mRNA expression, including molecular layer of CA1, cell body and molecular layers of the subiculum, and layer III of the entorhinal cortex (**Fig. 1f, g, Extended Data 3c, d**).

The hippocampal network includes extended projections from the subiculum to the anteroventral thalamus and the medial mammillary nucleus[32–36]. These projections also display targeting specificity within the medial and lateral hippocampal networks and can be highlighted by tracing from the *Lphn2*+ and *Ten3*+ regions of the subiculum (**Extended Data Fig. 4**). Double *in situ* hybridization for *Lphn2* mRNA and *Ten3* mRNA in the 'extended hippocampal network' target regions of P8 mice revealed that *Lphn2* and *Ten3* expression matched axonal projections from neurons in the *Lphn2*+ and *Ten3*+ subiculum regions (**Fig. 1h**). *Lphn2* showed enriched expression in the ventromedial area of the anteroventral thalamus and the medial part of the medial mammillary nucleus, coinciding with axon projection targets of proximal, *Lphn2*+ subiculum neurons. By contrast, *Ten3* was highly expressed in the dorsolateral portion of the anteroventral thalamus and the lateral part of the medial mammillary nucleus, coinciding with axon projection targets of distal, *Ten3*+ subiculum neurons (compare **Fig. 1h** with **Extended Data Fig. 4c, d**). Furthermore, expression of Lphn2 and Ten3 protein was consistent with mRNA expression in extended hippocampus target regions (**Fig. 1i**).

In summary, *Lphn2* and *Ten3* mRNA, as well as Lphn2 and Ten3 proteins, exhibit striking inverse expression within multiple regions of the developing extended hippocampal network, including CA1, subiculum, entorhinal cortex, anteroventral thalamus, and medial mammillary nucleus. In all cases, the connection specificity follows a 'Ten3→Ten3, Lphn2→Lphn2' rule (**Fig. 1j**).

Ten3+ CA1 axons avoid Lphn2+ targets

Ten3 directs targeting of pCA1→dSub axons through matching expression and homophilic attraction[5]. Does Lphn2 also act as a homophilic attractant to assemble the lateral hippocampal network? To determine

if Lphn2 promotes homophilic adhesion, we performed an *in vitro* cell aggregation assay using non-adhesive K562 cells. We found that Ten3-expressing K562 cells formed aggregates (**Extended Data Fig. 5a**) as previously reported[5], but Lphn2-expressing cells did not (**Extended Data Fig. 5b**). However, Lphn2-expressing cells aggregated with Ten3-expressing cells (**Extended Data Fig. 5c**), consistent with previously reported heterophilic interaction between Teneurins and Latrophilins[5,7,17,29,31]. The heterophilic interaction of Lphn2 and Ten3 combined with their striking complementary expression in lateral versus medial subnetworks suggests that the interaction between Lphn2 and Ten3 may result in repulsion, which could enhance the targeting precision of the lateral and medial hippocampal networks.

To determine if Lphn2 in target neurons repel Ten3+ axons, we interrogated the CA1→Sub connection. dCA1 and pCA1 axons extend along a tract above the subiculum cell body layer until they reach Lphn2+ pSub and Ten3+ dSub, respectively, where they invade the cell body layer of the subiculum to form synapses[5] (**Fig. 2a**). Because the CA1→Sub projection develops postnatally[5], we injected lentivirus (LV) expressing *GFP* (control) or *GFP-P2A-Lphn2* into the Lphn2-low dSub of mice at P0 to create a region of subiculum expressing Lphn2 across the entire proximal-distal axis. We then injected AAV encoding membrane-bound mCherry (*AAV-ChR2-mCh*) into pCA1 in these same mice as adults to label and trace Ten3+ CA1 axons (**Fig. 2b**). The portion of subiculum transduced by LV was only a subset of the total pCA1 axon targeting region, allowing us to determine if pCA1 axons target LV-transduced subiculum regions differently compared to neighboring non-LV-transduced subiculum regions. In *LV-GFP* controls, pCA1 axon targeting was unaffected in sections expressing GFP (**Fig. 2c**; **Extended Data Fig. 6a, d,** left panels). In contrast, in *LV-GFP-P2A-Lphn2* injected brains, pCA1 axons avoided regions where Lphn2 was overexpressed in dSub (**Fig. 2e**; **Extended Data Fig. 6b, e**, left panels). Deletion of the lectin binding domain in Latrophilins has been shown to abolish Teneurin binding while not affecting interactions with other known partners or surface expression[7,17,22,29]. Therefore, we overexpressed Lphn2_ΔLEC in the subiculum to determine if pCA1 avoidance depends on a Lphn2/Teneurin interaction. We found that in *LV-GFP-P2A-Lphn2_ΔLEC* injected brains pCA1 axons were not affected by regions expressing Lphn2_ΔLEC and displayed normal targeting to dSub (**Fig. 2g**; **Extended Data Fig. 6c, f**, left panels).

To further assess how Ten3+ axons target the subiculum in regions where Lphn2 is overexpressed, we generated 'mountain-plots,' where pCA1 axons (mCh+) and LV injection site (GFP+) intensities were plotted on the same graph as height and color, respectively. Overexpression of GFP alone did not affect the intensity of pCA1 axons targeting the subiculum (**Fig. 2d**; **Extended Data Fig. 6d**, right panels). However, pCA1 axon intensity was markedly reduced in regions overexpressing Lphn2 (**Fig. 2f**; **Extended Data Fig. 6e**, right panels), but not in regions overexpressing Lphn2_ΔLEC (**Fig. 2h**; **Extended Data Fig. 6f**, right panels). These gain-of-function experiments indicate that Ten3+ pCA1 axons avoid Lphn2+ subiculum target regions in a Lphn2/Teneurin interaction-dependent manner.

Ten3+ CA1 axons invade *Lphn2*$^{-/-}$ targets

To determine if Lphn2 in the subiculum is necessary for correct pCA1→dSub targeting, we performed a loss-of-function experiment by injecting *LV-GFP-Cre* into the subiculum of control and *Lphn2*$^{fl/fl}$ mice[31]

at P0, followed by *AAV-ChR2-mCh* in pCA1 of the same mice as adults to assess Ten3+ axon targeting (**Fig. 3a**). In *Lphn2*$^{+/+}$ control animals, pCA1 axons targeted dSub and were not disrupted when projecting into GFP-Cre+ expressing regions (**Fig. 3b** and **Extended Data Fig. 7a, e**, left panels). In contrast, Ten3+ pCA1 axons spread into the pSub of GFP-Cre+ regions in *Lphn2*$^{fl/fl}$ mice (**Fig. 3d** and **Extended Data Fig. 7b, f**, left panels). Semi-transparent mountain-plots collapsed on the medial-lateral axis revealed increased pCA1 axon intensity in the proximal portion of subiculum only in GFP-Cre+ regions of *Lphn2*$^{fl/fl}$ mice (**Fig. 3e** and **Extended Data Fig. 7f**, right panels), compared to *Lphn2*$^{+/+}$ mice (**Fig. 3c** and **Extended Data Fig. 7e**, right panels). Quantification of pCA1 axon intensity in GFP-Cre+ sections revealed that pCA1 axons covered a broader area of subiculum along the proximal-distal axis in *Lphn2*$^{fl/fl}$ mice compared to *Lphn2*$^{+/+}$ mice (**Fig. 3f, g**). Thus, Lphn2 in pSub target neurons normally repel Ten3+ pCA1 axons, enabling them to specifically target dSub.

To rule out the possibility that the ectopic invasion of pCA1 axons into *Lphn2*$^{-/-}$ pSub results from loss of Lphn2 interaction with a molecule other than Ten3 (e.g., another Teneurin that is expressed in pCA1), we performed the same *Lphn2* loss-of-function experiment in *Ten3*$^{-/-}$ mice. Anterograde tracing from pCA1 in *Lphn2*$^{+/+}$*;Ten3*$^{-/-}$ mice showed pCA1 axons spread more along the proximal-distal axis of the subiculum as previously reported[5] (**Fig. 3h, i**; **Extended Data Fig. 7c, g**). In *Lphn2*$^{fl/fl}$*;Ten3*$^{-/-}$ mice, pCA1 axons also showed more spreading along the proximal-distal axis of the subiculum, and the GFP-Cre+ regions no longer affected the pCA1 axon targeting patterns (**Fig. 3j, k**; **Extended Data Fig. 7d, h**). Furthermore, the projection width of axons in *Lphn2*$^{fl/fl}$*;Ten3*$^{-/-}$ mice was not significantly different from *Lphn2*$^{+/+}$*;Ten3*$^{-/-}$ mice (**Fig. 3l, m**). The lack of any additional axon mistargeting phenotype in *Lphn2*$^{fl/fl}$*;Ten3*$^{-/-}$ mice compared to *Lphn2*$^{+/+}$*;Ten3*$^{-/-}$ mice suggests that Ten3 is required for the effect of loss of subiculum Lphn2 on pCA1 axon targeting, and that Lphn2/Ten3-mediated repulsion directs precise pCA1→dSub targeting.

Repulsion and attraction cooperate

Loss of Lphn2/Ten3 heterophilic repulsion (**Fig. 3**) or Ten3 homophilic attraction[5] alone both disrupt precise pCA1→dSub axon targeting. What is the relative contribution of each? To test this, we simultaneously conditionally deleted both *Lphn2* and *Ten3* in the subiculum and assessed the targeting of Ten3+ pCA1 axons. We found that pCA1 axons projecting into GFP-Cre+ regions of *Lphn2*$^{fl/fl}$*;Ten3*$^{fl/fl}$ targeted more proximal regions of subiculum and also had decreased fluorescence intensity in distal subiculum (**Fig. 4a–c**; **Extended Data Fig. 8**). Quantification of pCA1 axons in GFP-Cre+ subiculum sections of *Lphn2*$^{fl/fl}$*;Ten3*$^{fl/fl}$ mice showed spreading into the *Lphn2*$^{-/-}$ pSub region similar to *Lphn2*$^{fl/fl}$*;Ten3*$^{+/+}$ mice, and additionally decreased fluorescence intensity in the *Ten3*$^{-/-}$ dSub region compared to *Lphn2*$^{fl/fl}$*;Ten3*$^{+/+}$ mice (**Fig. 4d**). The width of pCA1 axon projections in GFP-Cre+ *Lphn2*$^{fl/fl}$*;Ten3*$^{fl/fl}$ subiculum region was significantly larger than in wild type controls (**Fig. 4e**), confirming the loss of repulsion of pCA1 axons to Lphn2+ pSub. At the same time, the position of the projection peak shifted significantly more proximal in *Lphn2*$^{fl/fl}$*;Ten3*$^{fl/fl}$ compared to *Lphn2*$^{fl/fl}$*;Ten3*$^{+/+}$ mice (**Fig. 4f**), consistent with loss of attraction of Ten3+ pCA1 axons to Ten3+ dSub. Together, these data demonstrate that Lphn2/Ten3 heterophilic repulsion and Ten3/Ten3 homophilic attraction cooperate in orchestrating precise pCA1→dSub axon targeting; specifically, Lphn2 heterophilic repulsion prevents premature

innervation of Ten3+ pCA1 axons in pSub, whereas Ten3 homophilic attraction promotes Ten3+ pCA1 axons to innervate dSub (**Fig. 4g**).

Discussion

Cell surface proteins play important roles in many developmental processes. Heterophilic interactions between adhesion GPCR Latrophilins and type II transmembrane proteins Teneurins have been proposed to promote synaptic adhesion and axon attraction[12,22,30]. However, a recent study provided evidence for a repulsive Lphn1/Ten2 interaction in the context of neuronal migration[17]. Here, we provide several lines of evidence demonstrating that Lphn2 acts as a repulsive ligand for Ten3+ axons in the precise wiring of the hippocampal network. First, Lphn2 and Ten3 exhibit striking complementary expression in multiple nodes of the extended hippocampal network, following a 'Ten3→Ten3, Lphn2→Lphn2' rule (**Fig. 1**). Second, gain-of-function analysis revealed that Ten3+ pCA1 axons avoid dSub where Lphn2 is ectopically expressed (**Fig. 2**). Third, loss-of-function experiments revealed that Ten3+ pCA1 axons invade pSub devoid of *Lphn2* (**Fig. 3**). Thus, Lphn2 plays a critical role in circuit assembly preceding synapse formation. While defects in axon targeting may contribute to previously reported findings of synaptic deficits in *Latrophilin* loss-of-function experiments[22,31], our study does not rule out the possibility that Latrophilin/Teneurin interactions play additional roles in synaptic adhesion if the repulsive mechanism is switched off after axon targeting is complete.

The molecular mechanism underlying Lphn2/Ten3-mediated repulsion in axon targeting has yet to be fully elucidated. Both Latrophilins and Teneurins have been shown to undergo cleavage through autoproteolysis and proteolysis, respectively, of their extracellular domains[30,37]. It is conceivable that Lphn2-Ten3 binding, while sending a repulsive signal to Ten3+ growth cones, also triggers the cleavage of Ten3, Lphn2, or both molecules, thus terminating transient axon-target interaction. Alternatively, transient axon-target interaction could be terminated by endocytosis of the Lphn2/Ten3 complex. Both mechanisms have been reported in the context of the Ephrin/Eph receptor-mediated repulsion[38,39]. Intriguingly, the C-terminal intracellular domain of Latrophilin is reported to interact with TRIP8b, a clathrin-interacting protein involved in neuronal endocytosis[40,41]. In addition, Latrophilins are known to bind both Teneurins and Flrts, cell surface molecules that can function as a repulsive cue in both axon guidance and radial cell migration[42–44]. Interestingly, our transcriptomic analysis revealed that *Flrt2* has higher expression in *Ten3*-HIGH versus *Ten3*-NONE CA1 cells, suggesting that it may cooperate with Ten3 to increase Lphn2-dependent repulsion. However, this expression pattern is not maintained across subiculum and entorhinal cortex (**Extended Data Fig. 9a**).

Our results highlight the remarkable specificity of Latrophilin-Teneurin interactions. Deletion of *Lphn2* in the subiculum causes Ten3+ pCA1 axons to no longer be repelled from the pSub (**Fig. 3**), even though *Lphn1* is expressed at higher levels than *Lphn2* across all regions (**Extended Data Fig. 9b**), suggesting Lphn1 cannot compensate for the loss of Lphn2. Additionally, Ten2 and Ten4, which are highly expressed in CA1 neurons (**Extended Data Fig. 9c**), do not appear to compensate for the loss of Ten3 (**Fig. 3**). It is unclear whether distinct Latrophilin/Teneurin complexes have different interaction affinities or unique signaling mechanisms elicited by extracellular binding. Appreciating that different

isoform combinations of Latrophilin-Teneurin complexes may vary in function is critical to fully understanding the roles of these molecules in brain development and function.

A striking finding in this study is the complementary expression of *Lphn2* and *Ten3* across all regions of the MHN and LHN, respectively (**Fig. 1j**). This pattern of inverse expression suggests that Lphn2 and Ten3 may also be important for establishing the connectivity of seven additional projections that follow the 'Ten3→Ten3, Lphn2→Lphn2' rule. Furthermore, while we have demonstrated that Lphn2 acts as a repulsive ligand for Ten3+ axons in establishing connection specificity in the MHN network, it remains possible that Ten3 can act as a repulsive ligand for Lphn2+ axons, contributing to targeting specificity in the LHN network.

Finally, our findings highlight the cooperation of repulsion and attraction in the precise assembly of the hippocampal network. Cooperation of attraction and repulsion has been described at different stages of neuronal circuit assembly, involving different ligand/receptor interactions[9,11]. For example, guidance of commissural axons across the midline requires Netrin/DCC- and Sonic Hedgehog/Boc-mediated attraction, followed by Slit/Robo-mediated repulsion[45,46]. Laminar-specific neuron target choice in the mouse retina requires both Sema6a/PlexA4-mediated repulsion and cadherin-mediated attraction[47,48]. Here, we showed that target choice of pCA1 axons is determined by Lphn2/Ten3-mediated repulsion from pSub, followed by Ten3/Ten3-mediated attraction to dSub (**Fig. 4g**). This presents the first example, to our knowledge, where a single molecule (Ten3) acts as a receptor for both repulsive and attractive ligands in the same axon when controlling neuron target choice.

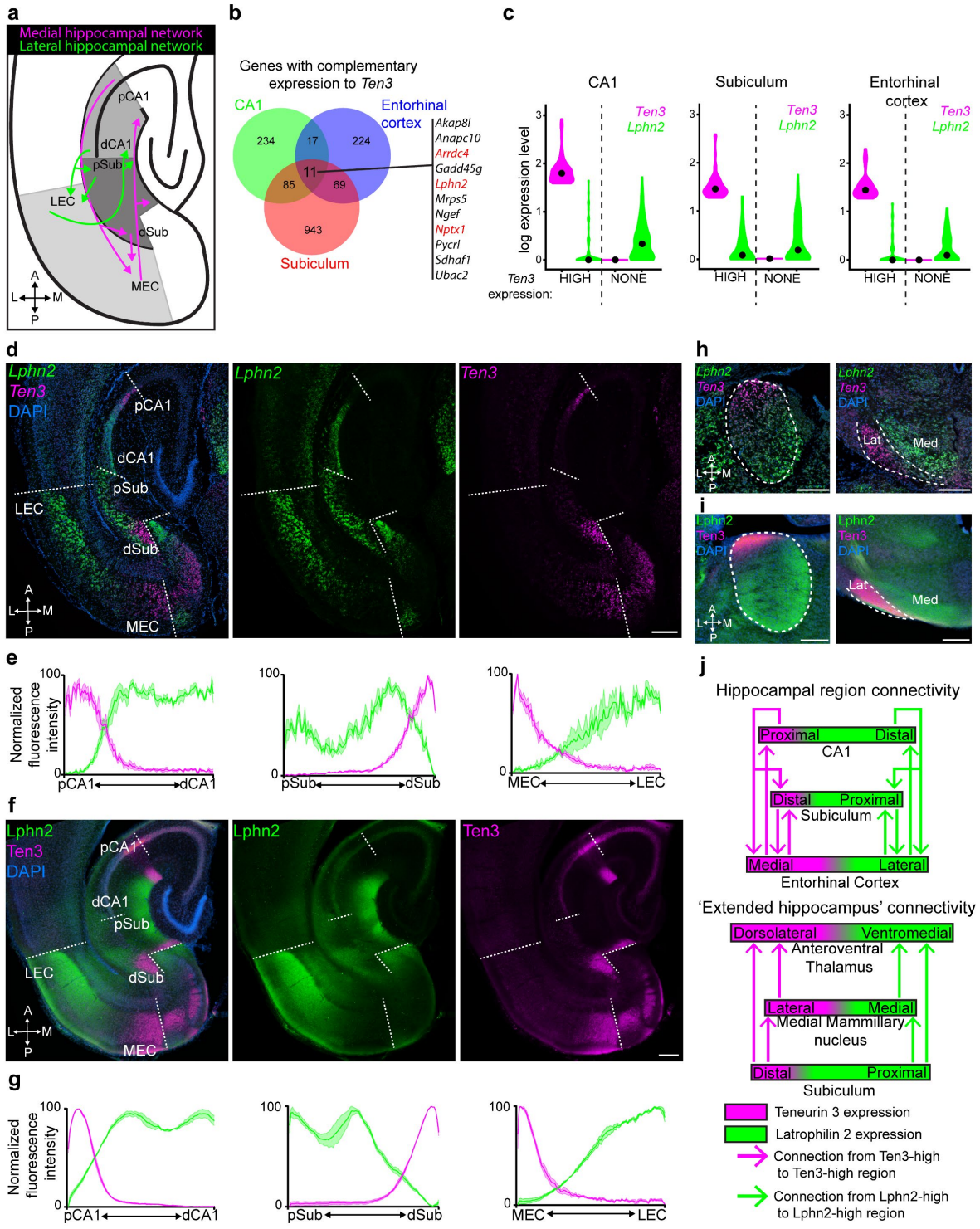

Fig. 1 | Lphn2 has complementary expression to Ten3 in the hippocampal network. a, Summary of axonal projection patterns of medial (magenta) and lateral (green) hippocampal network connections. A, anterior; P, posterior: L, lateral; M, medial. **b,** Venn diagram highlighting genes with complementary

expression to *Ten3* in CA1, subiculum, and entorhinal cortex. Eleven genes showed inverse expression to *Ten3* in all three regions. Highlighted in red are putative cell surface molecules. **c,** Violin plots highlighting *Lphn2* and *Ten3* expression in *Ten3*-HIGH and *Ten3*-NONE cells across CA1, subiculum, and entorhinal cortex. The unit of expression level is ln [1+ (reads per 10000)]. Black dots represent the median. **d,** Double *in situ* hybridization for *Lphn2* (middle) and *Ten3* (right) mRNA on a horizontal section of P8 mouse brain. Dashed lines represent boundaries between CA1, subiculum, and entorhinal cortex as labeled in the overlay (left). **e,** Quantification of *Lphn2* and *Ten3* mRNA across the proximal-distal axis of CA1 (*n*=3 mice, 29 sections total) and subiculum (*n*=3 mice, 31 sections total) cell body layers and the medial-lateral axis of layer III entorhinal cortex (*n*=3 mice, 22 sections total). Mean ± s.e.m. **f,** Double immunostaining for Lphn2 (middle; anti-GFP antibody in *Lphn2-mVenus* knock-in mice[31]) and Ten3 (right) on a horizontal section of P8 mouse brain. Dashed lines represent boundaries between CA1, subiculum, and entorhinal cortex as labeled in the overlay (left). **g,** Quantification of Lphn2 and Ten3 protein across the proximal-distal axis of molecular layers of CA1 (*n*=3 mice, 23 sections total) and subiculum (*n*=3 mice, 22 sections total), and the medial-lateral axis of layer III entorhinal cortex (*n*=3 mice, 14 sections total). Mean ± s.e.m. **h,** Double *in situ* hybridization showing *Lphn2* and *Ten3* mRNA expression in the anteroventral thalamus (left) and medial mammillary nucleus (right) of a P8 mouse. Lat: lateral; Med; medial. **i,** Double immunostaining for Lphn2 (left; anti-GFP antibody in *Lphn2-mVenus* knock-in mice[31]) and Ten3 on a P8 mouse brain, showing protein expression in anteroventral thalamus (left) and the medial mammillary nucleus (right). Dashed lines represent anteroventral nucleus (left) and the boundary between the medial and lateral regions of the medial mammillary nucleus (right) in both **h** and **i**. **j,** Schematic summary of the expression pattern of Lphn2 and Ten3 in relation to interconnected regions of the lateral and medial hippocampal networks. Scale bars, 200 μm.

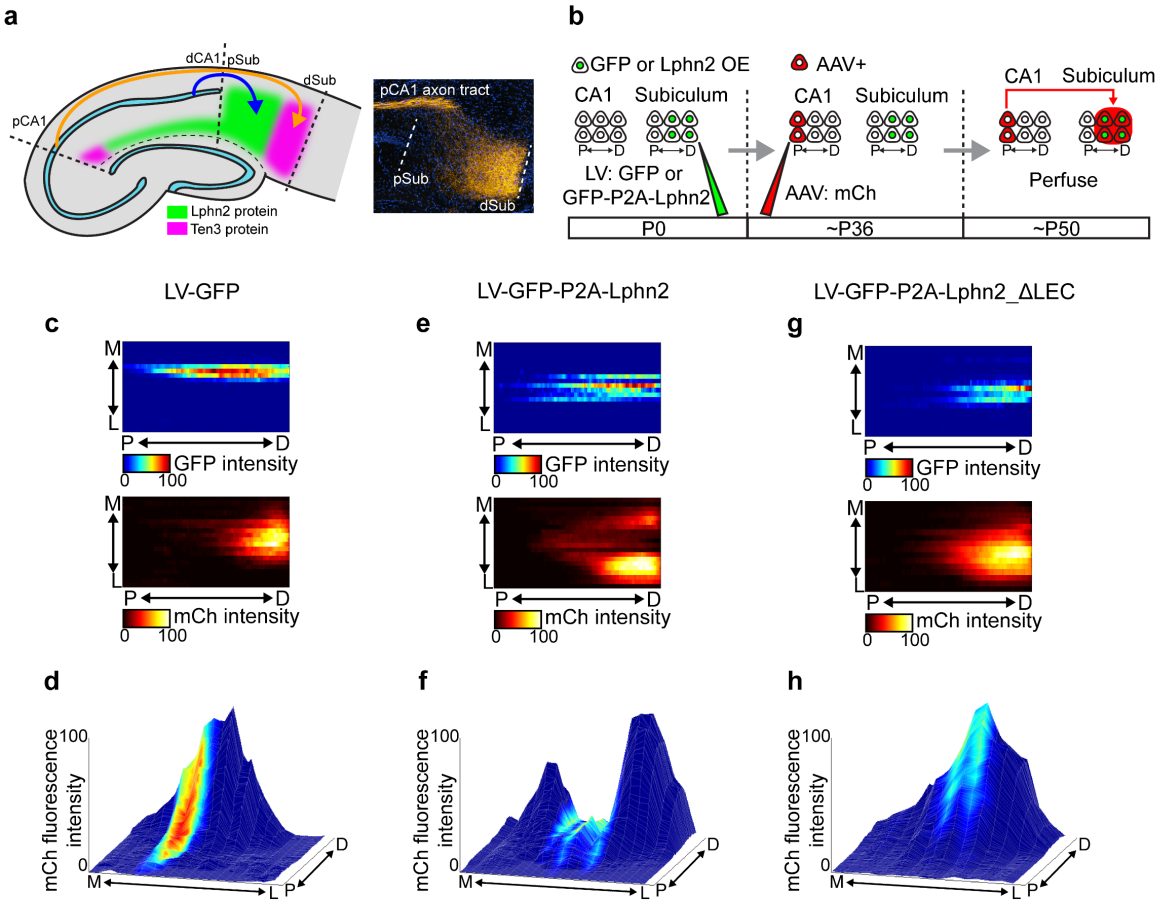

Fig. 2 | Ten3+ pCA1 axons avoid distal subiculum ectopically expressing Lphn2. a, Left, schematic diagram highlighting the trajectory of dCA1 (blue) and pCA1 (orange) axons to the subiculum. Right, confocal section of adult subiculum showing pCA1 axons (orange) extending along a tract above the subiculum cell body layer until they turn into dSub target area. **b,** Experimental design. **c, e, g,** Heatmaps showing normalized GFP fluorescence intensity (top) and normalized mCh fluorescence intensity (bottom) in subiculum. Each row is one section; adjacent sections are separated by 120 μm. **d, f, h,** Mountain-plots showing normalized GFP fluorescence intensity as color and normalized mCh fluorescence intensity as height. Same data as **c, e, g,** respectively. Lentiviral (LV) constructs injected are above each pair of panels. P, proximal; D, distal; M, medial; L, lateral.

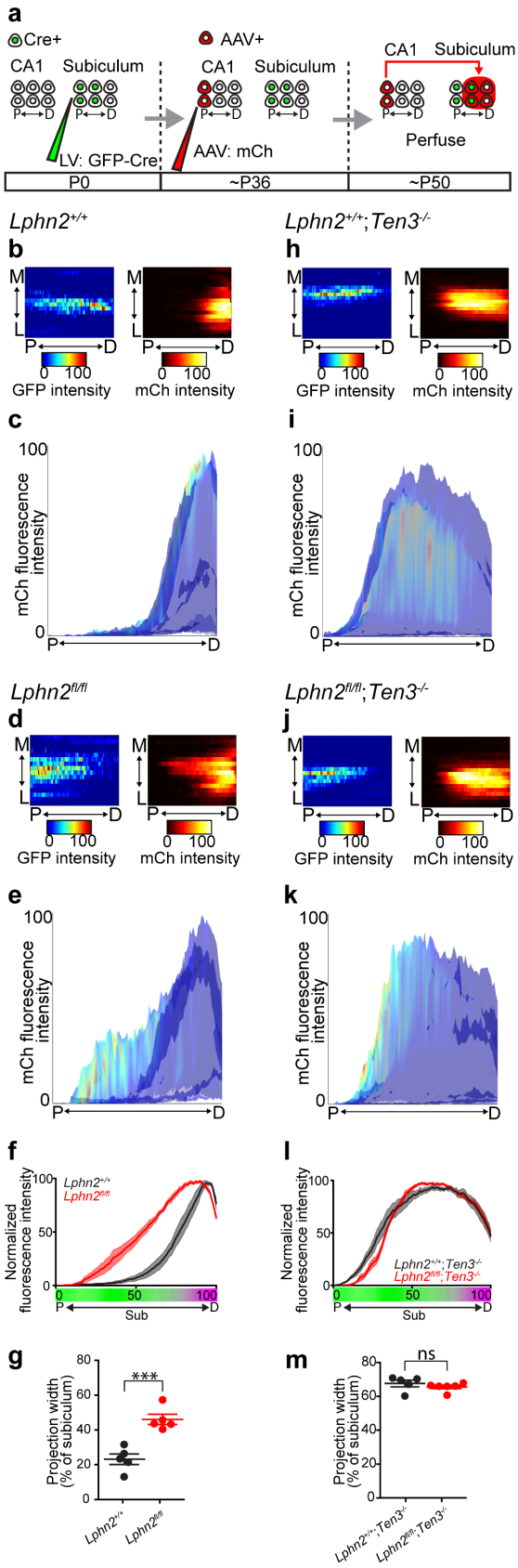

Fig. 3 | Ten3+ pCA1 axons invade pSub where *Lphn2* is deleted. a, Experimental design. **b, d, h, j,** Heatmaps showing normalized GFP-Cre fluorescence intensity (left) and normalized mCh fluorescence intensity (right) in subiculum. Each row is one section; adjacent sections are separated by 120 µm. Genetic conditions are as indicated above. **c, e, i, k,** Semi-transparent mountain-plots collapsed on the medial-lateral axis showing normalized GFP-Cre fluorescence intensity as color and normalized mCh fluorescence intensity as height. Same data as **b, d, h, j,** respectively. **f, l,** Averaged normalized mean fluorescence intensity traces of subiculum projections from pCA1 in GFP-Cre+ sections for $Lphn2^{+/+}$ (n=5 mice) and $Lphn2^{fl/fl}$ (n=5 mice) **(f)** and $Lphn2^{+/+};Ten3^{-/-}$ (n=5 mice) and $Lphn2^{fl/fl};Ten3^{-/-}$ (n=6 mice) **(l)**. Mean ± s.e.m**.** Color bar under x-axis represents Lphn2 (green) and Ten3 (magenta) expression in subiculum as quantified in Extended Data Fig. 3. **g, m,** Projection width-at-half-maximum for same data as **f, l**, respectively. ***, P=0.0006, ns = not significant, two-tailed t-tests. Error bars, mean ± s.e.m.

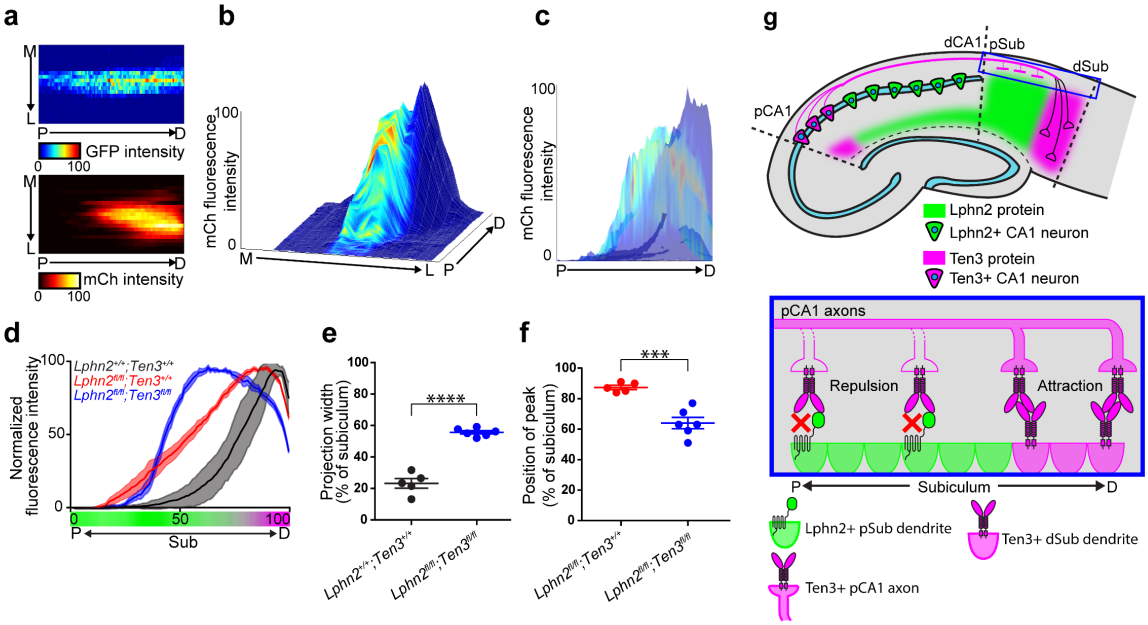

Fig. 4 | Simultaneous conditional deletion of *Lphn2* and *Ten3* in the subiculum reveals cooperation of Lphn2/Ten3 mediated repulsion and Ten3/Ten3-mediated attraction. a, Heatmaps showing normalized GFP-Cre fluorescence intensity (top) and normalized mCh fluorescence intensity (bottom) in subiculum. Each row is one section; adjacent rows are separated by 120 μm. **b,** Mountain-plot showing normalized GFP-Cre fluorescence intensity as color and normalized mCh fluorescence intensity as height. Same data as **a**. **c,** Semi-transparent mountain-plot collapsed on the medial-lateral axis showing normalized GFP-Cre fluorescence intensity as color and normalized mCh fluorescence intensity as height. Same data as **a**. **d,** Average normalized mean fluorescence intensity traces of subiculum projections in GFP-Cre+ sections for $Lphn2^{+/+};Ten3^{+/+}$ (n=5 mice), $Lphn2^{fl/fl};Ten3^{+/+}$ (n=5 mice), and $Lphn2^{fl/fl};Ten3^{fl/fl}$ (n=6 mice). Color bar under x-axis represents Lphn2 (green) and Ten3 (magenta) expression in subiculum as quantified in Extended Data Fig. 3. **e,** Projection width-at-half-maximum for same data as **d**. **f,** Projection peak position for same data as **d**. ****$P \leq 0.0001$, ***$P = 0.0004$, two-tailed t-tests. Error bars, mean ± s.e.m. **g,** Working model. See Discussion for details.

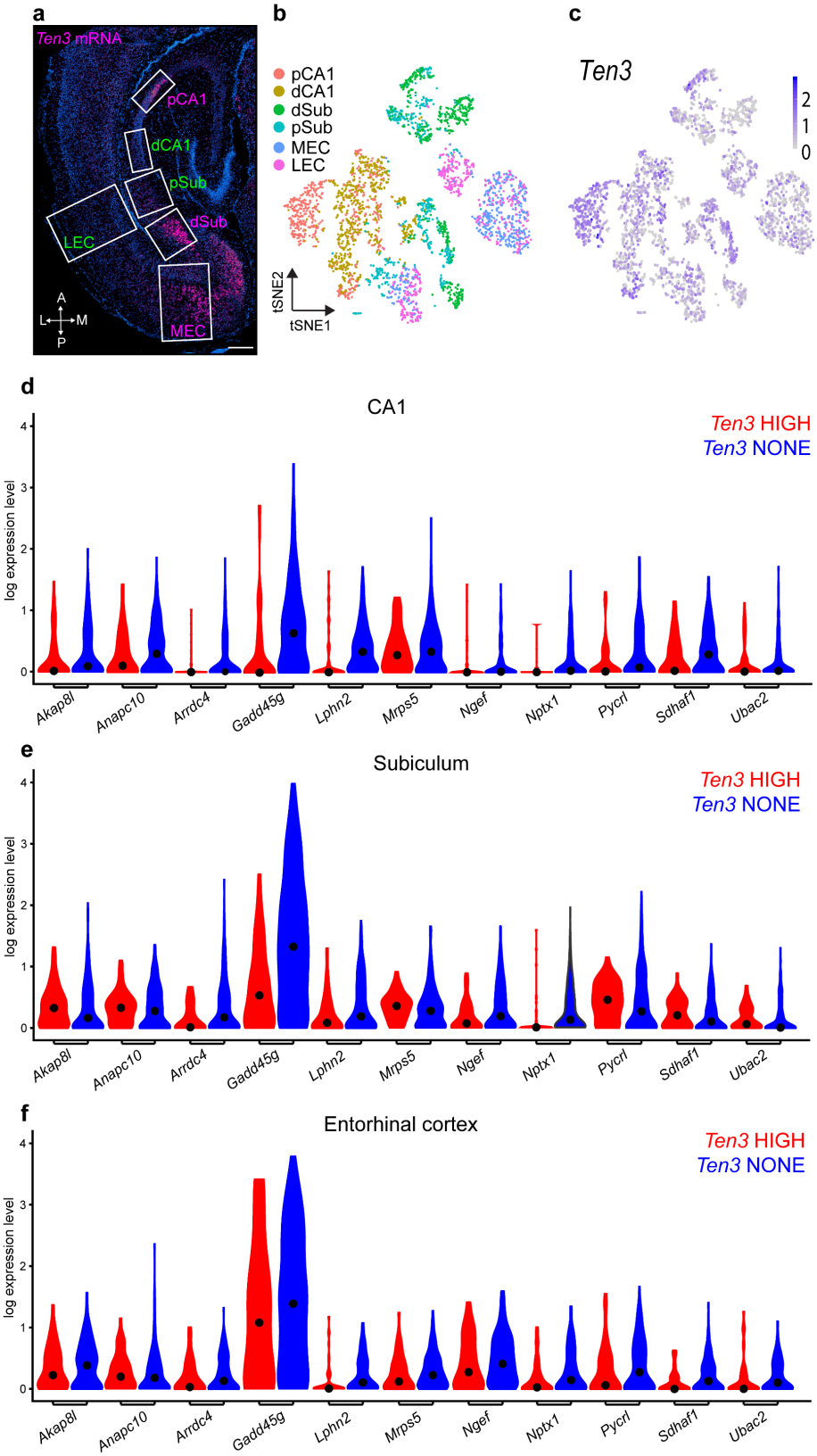

Extended Data Fig. 1 | Identifying genes with expression patterns complementary to *Ten3*. a, *In situ* hybridization for *Ten3* on a horizontal P8 mouse brain section with boxes labeling the regions of medial and lateral hippocampal network dissected for sequencing analysis. The boxed areas were micro-dissected, dissociated, and we performed fluorescence-activated cell sorting (FACS)-based single-cell RNA sequencing (scRNA-seq) using the Smart-Seq2 platform[49]. A, anterior; P, posterior: L, lateral; M, medial. Scale bar, 200 μm. **b,** tSNE plot of all sequenced cells labelled by dissected region. Identities of regions (color coded) are based on dissection and known molecular markers (Extended Data Fig. 2). **c,** *Ten3* expression represented on tSNE plot in **b**. Violin plots of all 11 genes showing inverse expression to *Ten3* across CA1 (**d**), subiculum (**e**), and entorhinal cortex (**f**). Unit of expression level is ln [1+ (reads per 10000)]. Black dots represent the median.

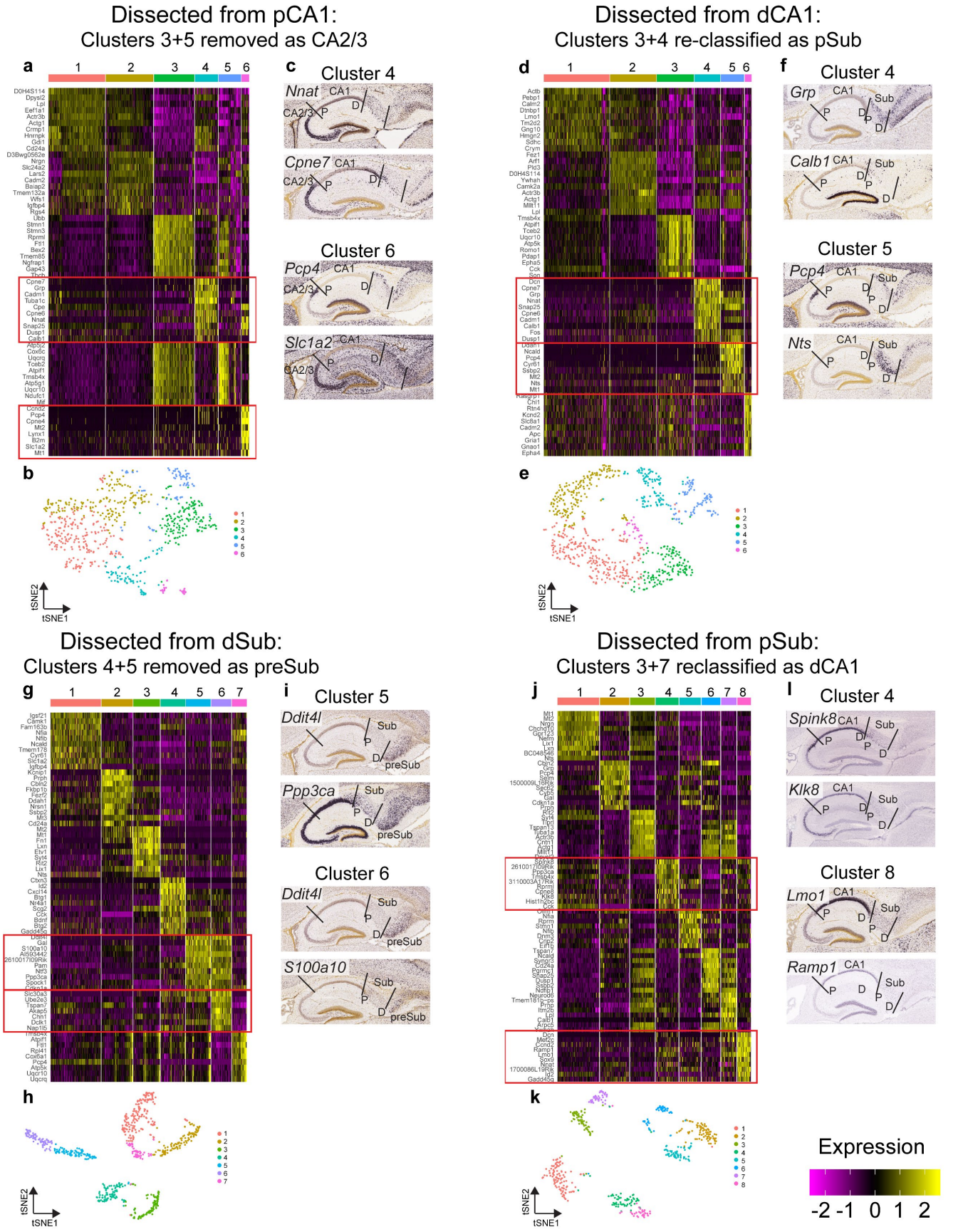

Extended Data Fig. 2 | Removal and re-classification of cells based on molecular markers. a, d, g, j, Heatmaps highlighting the top 10 differentially expressed genes in each cluster for the dissected regions pCA1, dCA1, dSub, pSub. LEC and MEC were not included here since no cells were removed or re-classified from these regions. Red boxes indicate the clusters that were removed, or re-classified based on molecular markers. **b, e, h, k,** tSNE plots of all sequenced cells in each dissected region, as indicated (see Methods). **c, f, i, l,** *In situ* hybridization images from Allen Institute website (www.mouse.brain-map.org)[50] highlighting the spatial expression of genes expressed in clusters that were removed or re-classified. More specifically, we examined the spatial expression pattern of the top 10 genes in each cluster using the *in situ* hybridization images from Allen Institute website[50]. All clusters except those highlighted (**a**), (**d**), (**g**), and (**j**) expressed molecular markers that corresponded to the region of dissection. In the pCA1 dissection (**a–c**), clusters 4 and 6 displayed enriched expression for genes present in CA2/3 and not CA1. Clusters 4 and 6 were thus removed before analysis. In the dCA1 dissection (**d–f**), clusters 4 and 5 displayed enriched expression for genes present in subiculum and not CA1, likely due to the close proximity of dCA1 to pSub. Clusters 4 and 5 were thus re-classified as pSub cells before analysis. In the dSub dissection (**g–i**), clusters 5 and 6 displayed enriched expression for genes present in presubiculum and not subiculum. Clusters 5 and 6 were thus removed before analysis. In the pSub dissection (**j–l**), clusters 4 and 8 displayed enriched expression for genes present in CA1 and not subiculum, likely due to the close proximity of pSub to dCA1. Clusters 4 and 8 were thus re-classified as dCA1 cells before analysis. All the *in situ* hybridization images presented here are from P14 mice, except for *Spink8*, *Klk8* and *Ramp1*, which are from P56 mice because there is no data available for these genes at P14.

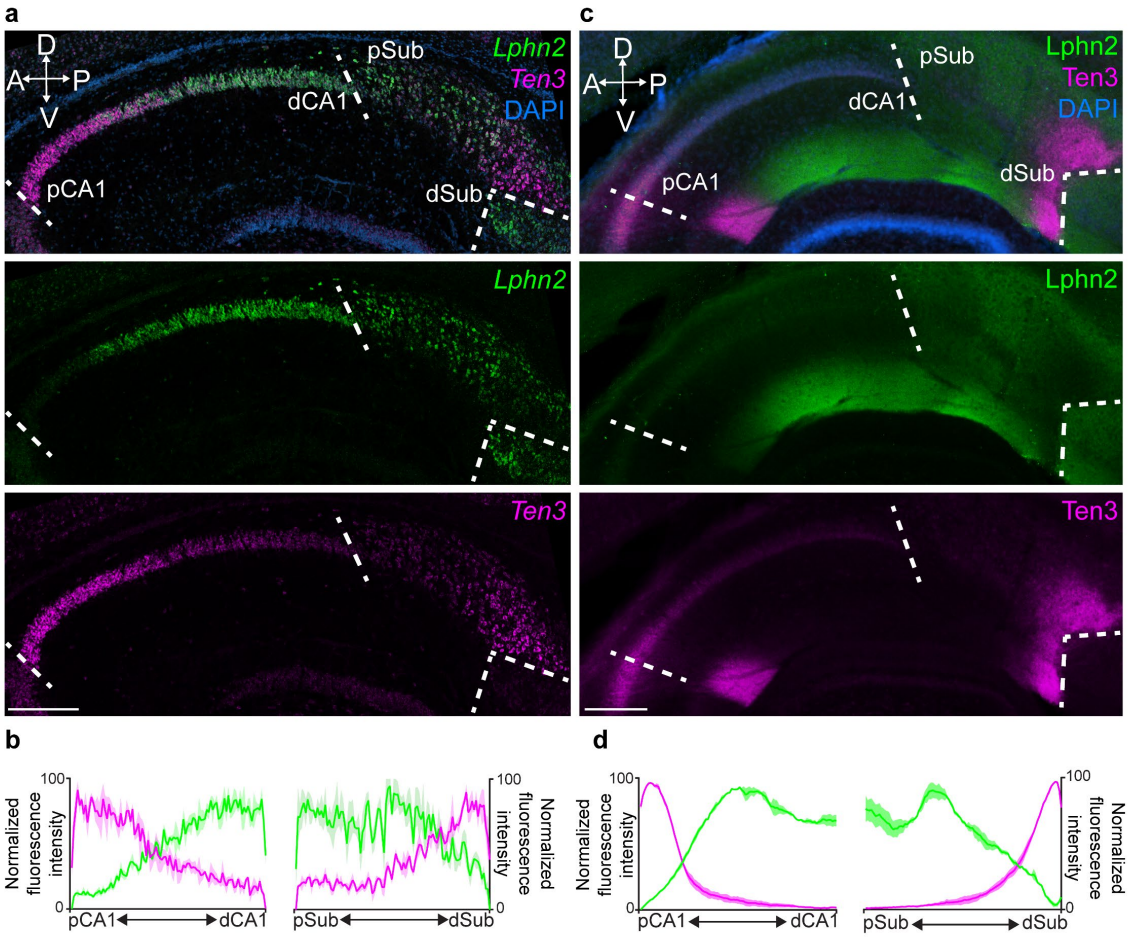

Extended Data Fig. 3 | Complementary expression patterns of *Lphn2* and *Ten3* in sagittal sections. **a,** Double *in situ* hybridization for *Lphn2* (middle) and *Ten3* (bottom) mRNA on a sagittal section of P8 mouse brain. Dashed lines represent boundaries between CA1 and subiculum as labeled in the overlay (top). A, anterior; P, posterior: D, dorsal; V, ventral. **b**, Quantification of *Lphn2* and *Ten3* mRNA across the proximal-distal axis of CA1 (*n* =3 mice, 23 sections total) and subiculum (*n* =3 mice, 19 sections total) cell body layers. Mean ± s.e.m. **c,** Double immunostaining for Lphn2 (middle; anti-GFP antibody in *Lphn2-mVenus* knock-in mice[31]) and Ten3 (bottom) on a sagittal section of P8 mouse brain. Dashed lines represent boundaries between CA1 and subiculum as labeled in the overlay (top). **d,** Quantification of Lphn2 and Ten3 protein across the proximal-distal axis of CA1 (*n* =2 mice, 20 sections total) and subiculum (*n* =2 mice, 20 sections total). Mean ± s.e.m. Scale bars, 200µm.

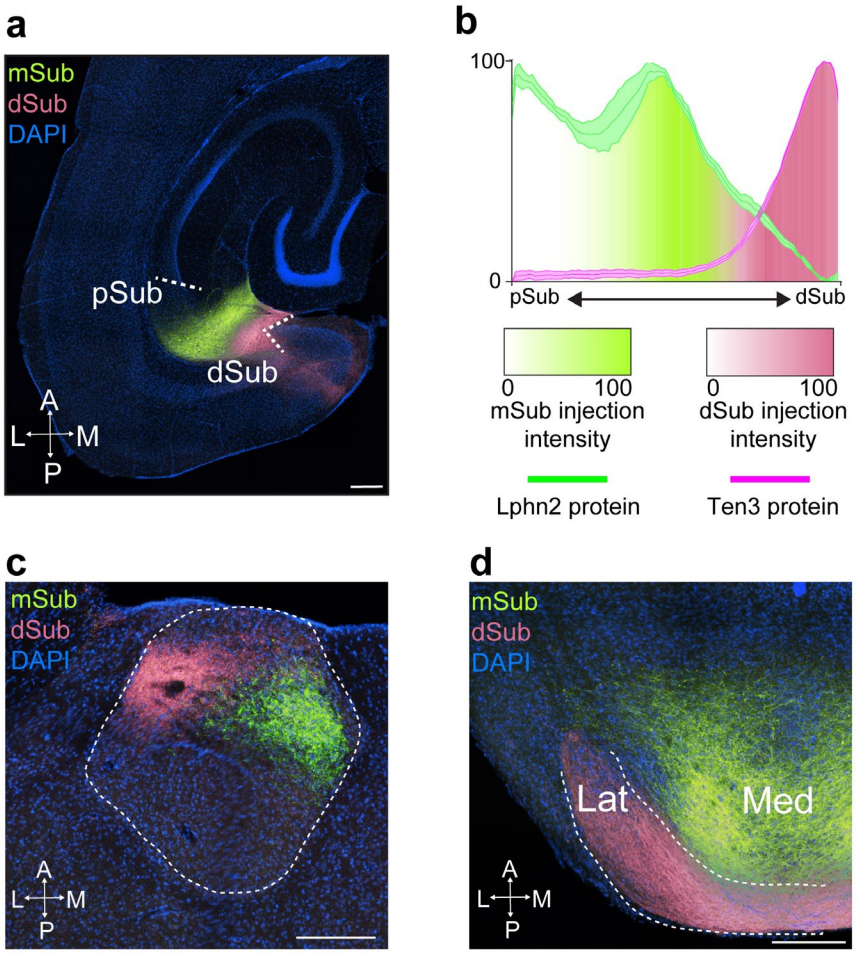

Extended Data Fig. 4 | Anterograde tracing from subiculum. a, Injection sites of dual anterograde tracing from Lphn2+ mid subiculum (mSub) and Ten3+ dSub in a P55 mouse brain. **b**, Quantification of injection sites position along the proximal-distal axis (intensity shown as color gradients) superimposed on Lphn2 and Ten3 protein distribution (curves) as shown in Fig. 1g. **c,** Projection of subiculum axons from (**a**) in the anteroventral nucleus of the thalamus. Lphn2+ axons target the medial region of the anteroventral thalamus, whereas Ten3+ axons target the lateral region. **d**, Projection of subiculum axons from (**a**) in the medial mammillary nucleus. Lphn2+ axons target the medial regions, whereas Ten3+ axons target the lateral region. A, anterior; P, posterior; L, lateral; M, medial. Scale bars, 200 μm.

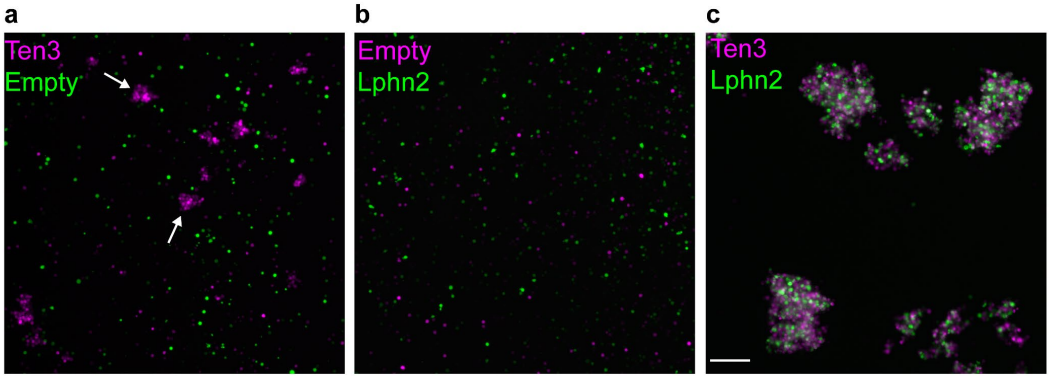

Extended Data Fig. 5 | Testing Ten3 and Lphn2 in promoting *trans*-cellular interactions. a, Non-adherent K562 cells transfected with Ten3/RFP, or GFP alone (empty), were mixed together. Ten3/RFP-expressing cells form aggregates (arrows), whereas GFP-expressing cells do not, confirming that Ten3 promotes homophilic adhesion[5]. **b,** K562 cells transfected with RFP alone (empty), or Lphn2/GFP, were mixed together. Neither cell populations form aggregates, suggesting that Lphn2 does not promote homophilic adhesion. **c,** K562 cells transfected with Ten3/RFP, or Lphn2/GFP, were mixed together. GFP- and RFP-expressing cells form aggregates, confirming Ten3 and Lphn2 mediate heterophilic adhesion[5,7,17,29,31]. Scale bar, 200 μm.

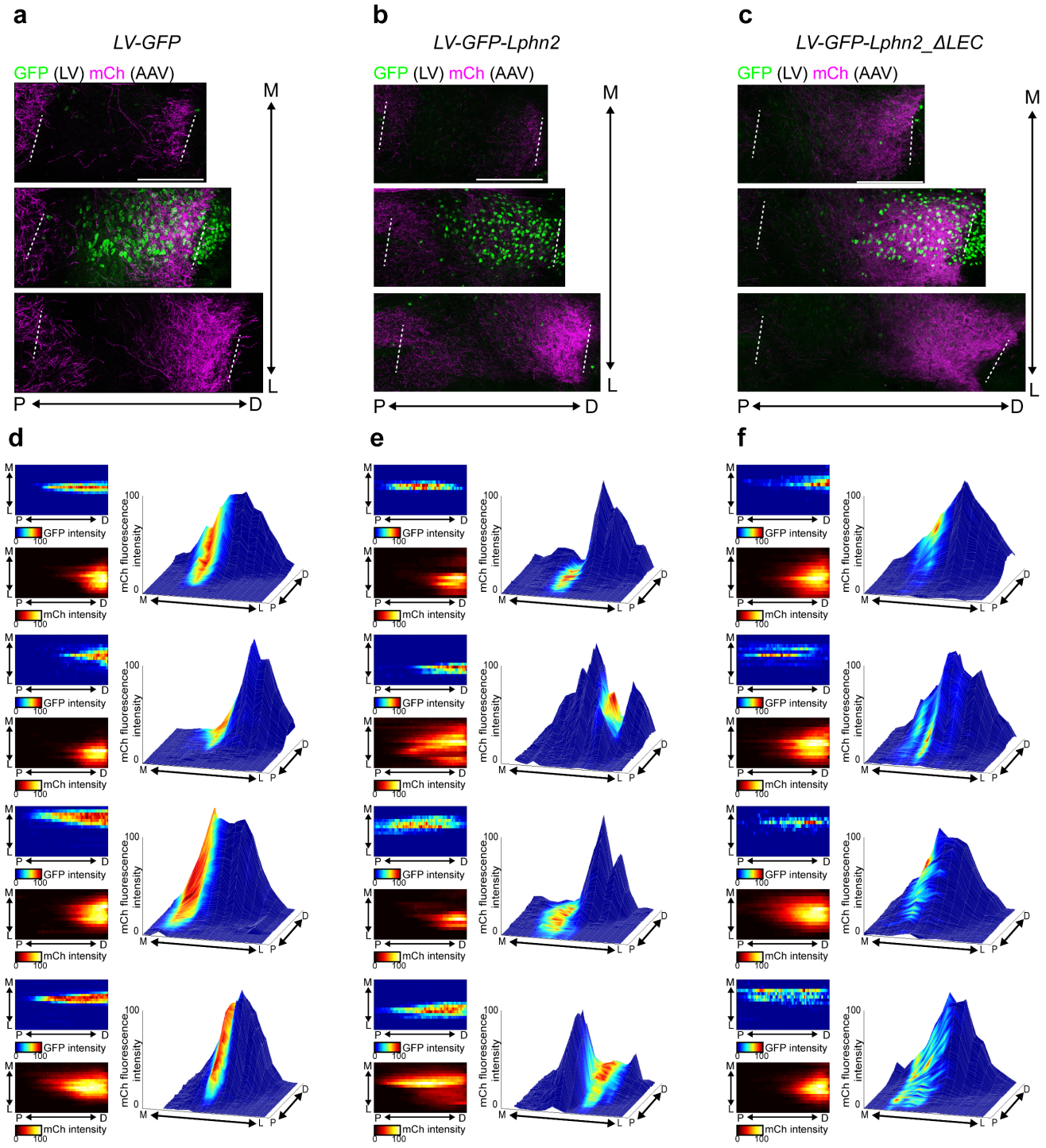

Extended Data Fig. 6 | Additional data related to Lphn2 gain-of-function experiments (Fig. 2). a, b, c, Example images from mice injected with *LV-GFP* (**a**), *LV-GFP-P2A-Lphn2_FLAG* (**b**) and *LV-GFP-P2A-Lphn2_ΔLEC_FLAG* (**c**), showing pCA1 axons (magenta) and LV (green) in subiculum. Three 60-µm sections that contain pCA1 axons at different positions along the medial–lateral (M–L) axis are shown, with the center one overlapping with the LV injection site. These images correspond to mice analyzed in

Fig. 2. Scale bars, 200 μm. **d, e, f,** Heatmaps and mountain plots from additional mice injected with *LV-GFP* (**d**), *LV-GFP-P2A-Lphn2_FLAG* (**e**), and *LV-GFP-P2A-Lphn2_ΔLEC_FLAG* (**f**) and analyzed as in Fig. 2c–h. Scale bars, 200μm.

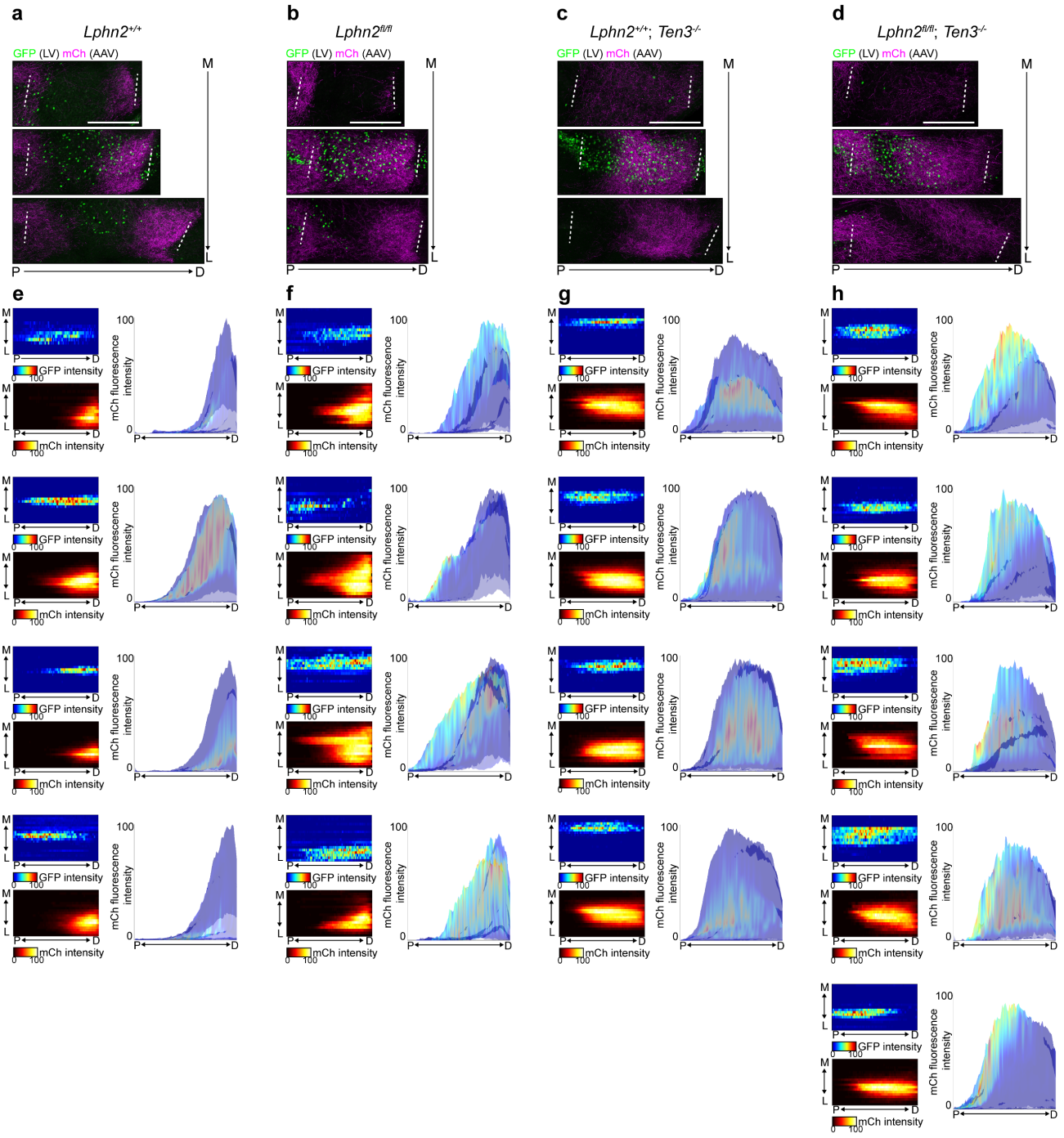

Extended Data Fig. 7 | Additional data related to the *Lphn2* conditional knockout experiment (Fig. 3). a–d Example images from *Lphn2*$^{+/+}$ (**a**), *Lphn2*$^{fl/fl}$ (**b**) and *Lphn2*$^{+/+}$*;Ten3*$^{-/-}$ (**c**) and *Lphn2*$^{fl/fl}$*;Ten3*$^{-/-}$ (**d**) mice injected with *LV-GFP-Cre* in subiculum, showing pCA1 axons (magenta) and LV (green) in subiculum. Three 60-µm sections that contain pCA1 axons at different positions along the medial–lateral (M–L) axis are shown, with the center one overlapping with the LV injection site. These images correspond to mice analyzed in Fig. 3. **e–h,** Heatmaps and mountain plots from additional *Lphn2*$^{+/+}$ (**e**),

Lphn2$^{fl/fl}$ (**f**) and *Lphn2*$^{+/+}$*;Ten3*$^{-/-}$ (**g**) and *Lphn2*$^{fl/fl}$*;Ten3*$^{-/-}$ (**h**) mice injected with *LV-GFP-Cre* and analyzed as in Fig. 3b–k and analyzed as in Fig. 3l, m. The variability of *LV-GFP-Cre* injection sites across the medial-lateral axis in subiculum accounts for the variation in the shape of the mountain plots, and depends on the axon intensity in the regions where LV injections site and AAV projections overlap. In *Lphn2*$^{fl/fl}$ animals (**f**), the region of axon spreading proximally in subiculum corresponds to the *LV-GFP-Cre* injection site, no matter its position across the medial-lateral axis. In *Lphn2*$^{fl/fl}$*;Ten3*$^{-/-}$ animals (**h**) there is no change in projection shape no matter the position of the *LV-GFP-Cre* injection site and the overall projection pattern is similar to *Lphn2*$^{+/+}$*;Ten3*$^{-/-}$ animals (**g**). Scale bars, 200 μm.

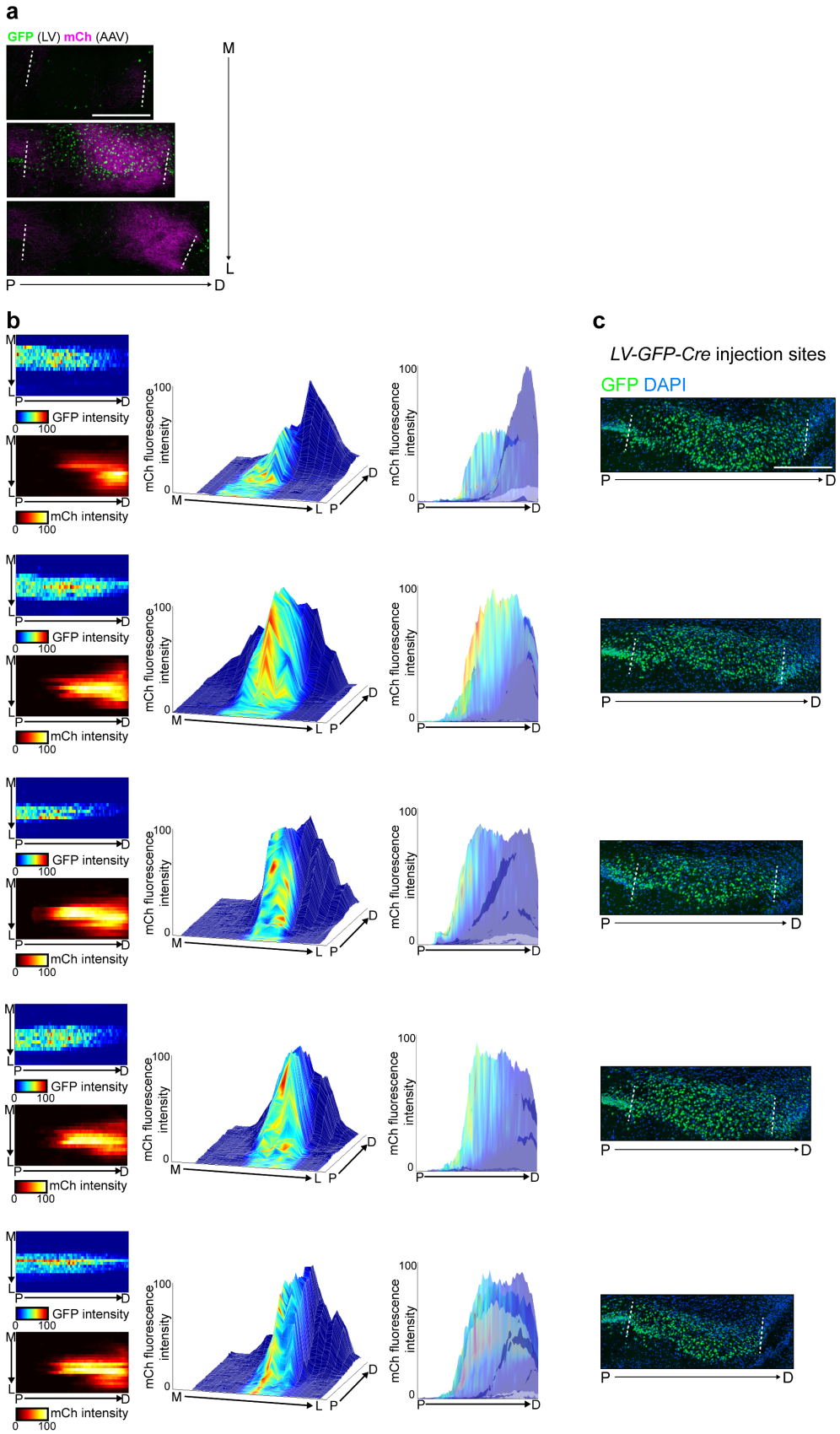

Extended Data Fig. 8 | Additional data related to double conditional knockout of *Lphn2* and *Ten3* (Fig. 4). a, Example images from *Lphn2*$^{fl/fl}$*;Ten3*$^{fl/fl}$ mouse injected with *LV-GFP-Cre*, showing pCA1 axons (magenta) and LV (green) in subiculum. Three 60-µm sections that contain pCA1 axons at different positions along the medial–lateral (M–L) axis are shown, with the center one overlapping with the LV injection site. These images correspond to the mouse in Fig. 4. **b,** Heatmaps and mountain plots from additional *Lphn2*$^{fl/fl}$*;Ten3*$^{fl/fl}$ mice injected with *LV-GFP-Cre* and analyzed as in Fig. 4a–c. The variability of *LV-GFP-Cre* injection sites across the medial-lateral axes in subiculum accounts for the variation in the shape of the mountain plots, and depends on the axon intensity in the regions where LV injections site and AAV projections overlap. In animals where the *LV-GFP-Cre* injection site is present in the first half of the medial-lateral axis (top panel), two clear peaks are present; the peak that has increased proximal spreading and decreased intensity in dSub corresponding with the *LV-GFP-Cre* and the peak that has no pSub spreading and highest axon intensity in the dSub corresponding with the region lacking *LV-GFP-Cre*. In other animals the *LV-GFP-Cre* injections site is present in the middle of the medial-lateral axis (second form top panel) and overlaps with the highest region of axon intensity. In this case only one peak is present, but these axons have spread further proximally in subiculum and their fluorescence intensity decreases in dSub. Therefore, the same effect is observed regardless of the position of the *LV-GFP-Cre* injection site across the medial-lateral axis, as can be seen in the quantification in Fig. 3d. **c,** Representative images of the *LV-GFP-Cre* injection site for each animal in (**b**). Increased GFP intensity in pSub results in low colormap signal in the dSub even though the density of GFP+ cells in dSub is high. Dotted lines define subiculum boundaries. Scale bars, 200 µm.

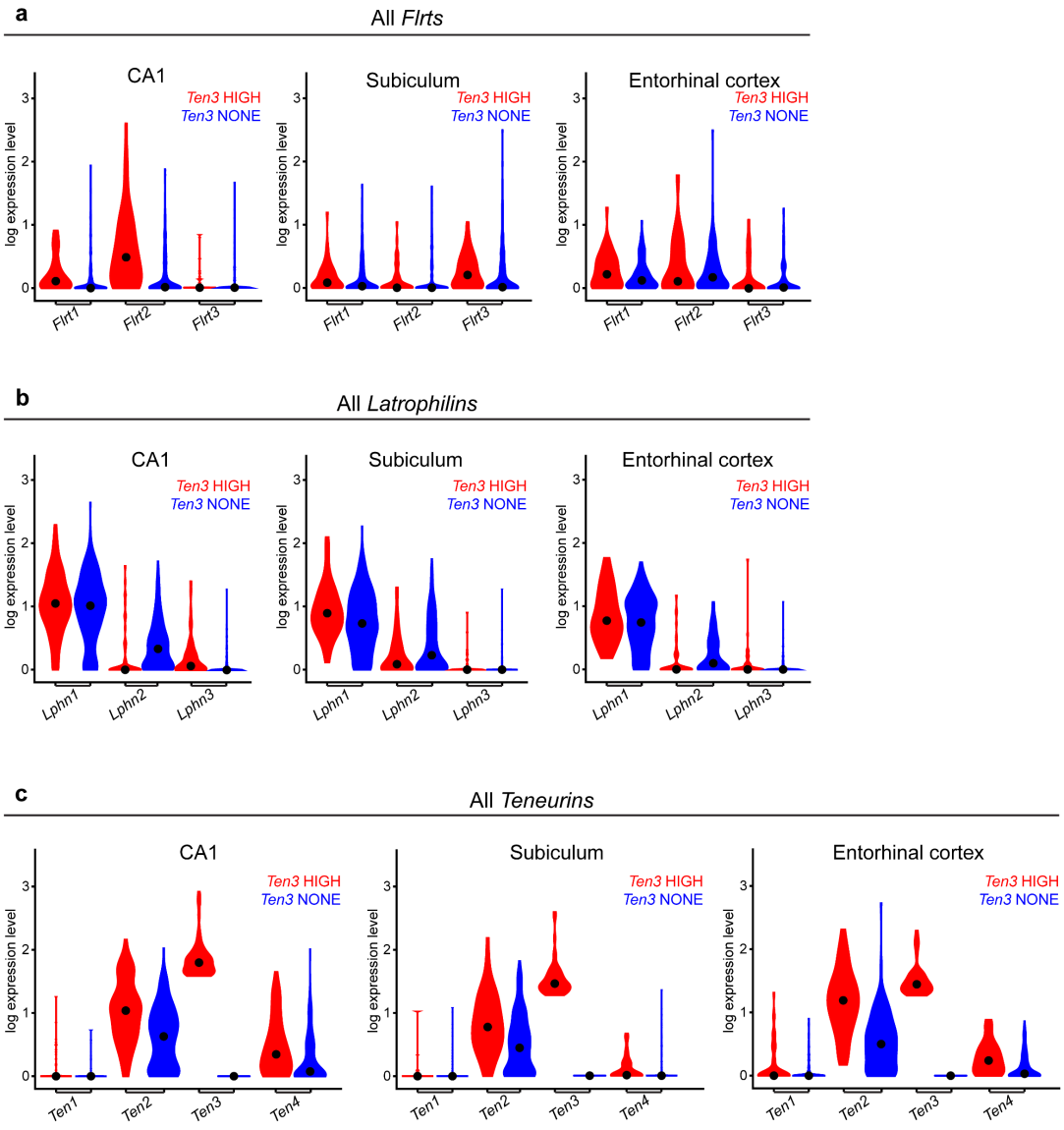

Extended Data Fig. 9 | Expression patterns of *Flrts*, *Latrophilins*, and *Teneurins* in the hippocampal network. Violin plots of *Flrts* (**a**), *Latrophilins* (**b**) and *Teneurins* (**c**) showing expression in *Ten3*-HIGH and *Ten3*-NONE cells across CA1, subiculum, and entorhinal cortex. Unit of expression level is ln [1+ (reads per 10000)]. Black dots represent the median. Cells were grouped based on *Ten3* levels (*Ten3*-HIGH or *Ten3*-NONE). *Flrt1, Flrt2,* and *Flrt3* did not show any consistent expression across all regions in *Ten3*-HIGH or *Ten3*-NONE cells. However, *Flrt2* did show enriched expression in *Ten3*-HIGH CA1 neurons. *Lphn1* showed a high level of expression in both *Ten3*-HIGH and *Ten3*-NONE neurons in CA1, subiculum and entorhinal cortex. *Lphn3* had low levels of expression in all cells across all regions. *Ten1* had low levels of expression in all cells across CA1, subiculum and entorhinal cortex. *Ten2* and *Ten4* showed higher levels of expression in *Ten3*-HIGH cells versus *Ten3*-NONE cells in CA1, subiculum and entorhinal cortex.

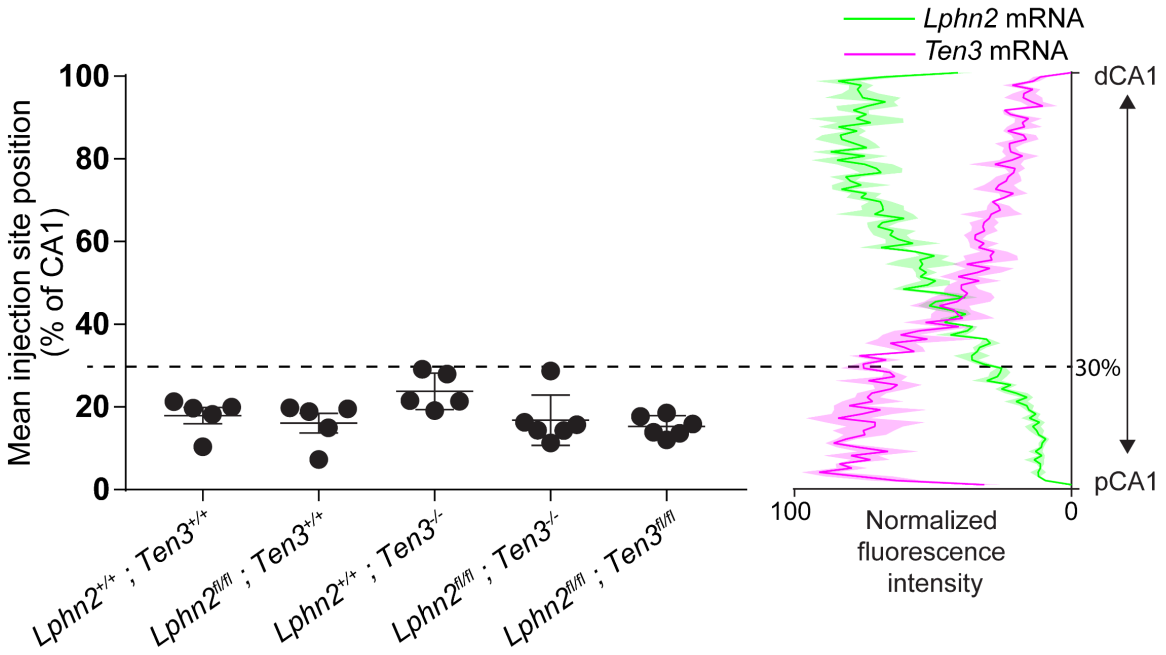

Extended Data Fig. 10 | Mean injection site position of pCA1 injections in animals from Figs. 2–4. All injections sites are located in the most proximal 30% of pCA1, which is the Ten3-high region of CA1 as determined by *in situ* hybridization quantification on sagittal P8 brain sections (from Extended Data Fig. 3).

Methods

Statistical analysis. Statistical tests were performed using GraphPad Prism 7. No statistical methods were used to determine sample size. Due to the low probability of correctly matching P0 lentivirus and adult AAV injections, all breeder pairs were homozygous, and therefore the experiments were not randomized. Due Images of aggregation assay (Extended Data Fig. 5), double AAV tracing (Extended Data Fig. 4) and Ten3 and Lphn2 immunostaining (Fig. 2e, f) are representative of at least three individual experiments. For *Lphn2* gain- and loss-of-function experiments (Figs. 3, 4, 5), results from all experiments are shown in Extended Data Figs. 6, 7, 8. See 'Image and data analysis for CA1 axon tracing' section for inclusion criteria.

Mice. All procedures followed animal care and biosafety guidelines approved by Stanford University's Administrative Panel on Laboratory Animal Care and Administrative Panel on Biosafety in accordance with NIH guidelines. Both male and female mice were used, and mice were group housed with access to food and water *ad libitum*. Sequencing experiments used mice heterozygous for *Vglut1-Cre*[51] (C57BL/6, and 129 background) and *Ai14*[52] (*Rosa-CAG-LSL-tdTomato-WPRE*, C57BL/6J background). CD-1 mice from Charles River Laboratories were used for double *in situ* hybridization, Lphn2 overexpression, and double AAV tracing studies. *Ten3*$^{-/-}$ mice[18] were maintained on the CD-1 background. *Lphn2*^{mVenus} and *Lphn2*$^{fl/fl}$ mice[31] were on a C57BL/6 and 129 mixed background and were backcrossed once onto the CD-1 background to improve pup survival rate. *Ten3*$^{fl/fl}$ mice[5] were on a mixed CD-1, C57BL/6, and 129 background and were backcrossed once onto a CD-1 background to improve pup survival rate. All genotyping was performed as previously described[5,18,31]. The total number of animals injected and screened for each experiment is as follows: **Fig. 2**: *LV-GFP*, 131; *LV-GFP-Lphn2*, 84; *LV-GFP-Lphn2_ΔLEC*, 126; **Fig. 3**: *Lphn2*$^{+/+}$, 176, *Lphn2*$^{fl/fl}$, 126, *Lphn2*$^{+/+}$*;Ten3*$^{-/-}$, 30, *Lphn2*$^{fl/fl}$*;Ten3*$^{-/-}$, 40; and **Fig. 4**: *Lphn2*$^{fl/fl}$*;Ten3*$^{fl/fl}$, 112.

Single cell sequencing. To express tdTomato in excitatory projection neurons for sequencing, mice heterozygous for *Vglut1-Cre* and *Ai14* were sacrificed at P8 for single cell isolation and sequencing. The following numbers of animals were used for each dissected regions: pCA1, 6 (3 rounds of isolation, 2 animals each isolation), dCA1, 4 (2 rounds of isolation, 2 animals each isolation), MEC 2, (1 round of isolation, 2 animals each isolation), LEC, 2 (1 round of isolation, 2 animals each isolation), dSub, 2 (1 round of isolation, 2 animals each isolation) and pSub, 2 (1 round of isolation, 2 animals each isolation). A total of 18 mice including both sexes were used in sequencing experiments.

To isolate tdTomato+ cells for single-cell sequencing, animals were briefly anesthetized with isoflurane and decapitated, and the brain was isolated in ice-cold ACSF (2.5 mM KCl, 7 mM $MgCl_2$, 0.5 mM $CaCl_2$, 1.3 mM NaH_2PO_4, 110 mM choline chloride, 25 mM $NaHCO_3$, 1.3 mM sodium ascorbate, 20 mM glucose, 0.6 mM sodium pyruvate, bubbled in 95% O_2 / 5% CO_2). Brains were embedded in 3% low-melting point agarose (Fisher BP165-25) in ACSF at 37 °C, cooled to 4 °C, and then cut on a vibratome into 350-µm floating sections. For CA1 and subiculum dissections, sections were cut on the sagittal plane; for entorhinal cortex dissections, sections were cut on the horizontal plane. Next, we visualized the fluorescent tdTomato labeling and used the atlas as a guide, to cut out the regions of interest as accurately

as possible. Microdissected tissue was incubated at 37 °C in papain enzyme mix + 800 nM kyneurenic acid (Worthington) for 30 minutes and triturated gently with a P200 pipette every 15 minutes thereafter until fully dissociated, usually within 1 hour of total incubation time. The cell suspension was spun down at 350 *g* for 10 min at room temperature, neutralized with ovomucoid inhibitor, spun again, washed in ACSF, stained with Hoechst for 10 minutes (1:2000, Life Technologies: H3570), washed, filtered (Falcon 532235), and resuspended in 2 mL ACSF. FACS was performed using the Sony SH800 system with a 130-µm nozzle suitable for the large size of excitatory neurons. Singlet cells were selected based on low FSC-W, and gated on Hoechst (nuclear stain that penetrates cell membrane) and tdTomato double positivity to identify labeled healthy neurons. Cells fulfilling these criteria were over 100× brighter than background, and were unambiguously identifiable. Single cells were sorted at a low flow rate (<100 events/second), and at the highest purity setting (Single Cell) into 384-well hard shell PCR plates (BioRad HSP3901) containing 0.4 µl lysis buffer [0.5 U Recombinant RNase Inhibitor (Takara Bio, 2313B), 0.0625% TritonX-100 (Sigma, 93443-100ML), 3.125 mM dNTP mix (Thermo Fisher, R0193), 3.125 µM Oligo-dT$_{30}$VN (Integrated DNA Technologies, 5′AAGCAGTGGTATCAACGCAGAGTACT$_{30}$VN-3′) and 1:600,000 ERCC RNA spike-in mix (Thermo Fisher, 4456740)] in each well, respectively. Following FACS, plates were spun down, sealed and stored at –80 °C. cDNA synthesis and library preparation protocols were adapted from the SMART-Seq2 protocol[49] (384-well processing utilized 0.4 µl starting volumes, and will hereafter be referred to as 1 unit. Plates were first thawed on ice followed by primer annealing (72 °C, for 3 minutes, then on ice). For reverse transcription, 1.5 units of reaction mix [16.7 U/µL SMARTScribe Reverse Transcriptase (Takara Bio, 639538), 1.67 U/µL Recombinant RNase Inhibitor (Takara Bio, 2313B), 1.67× First-Strand Buffer (Takara Bio, 639538), 1.67 µM TSO (Exiqon, 5′-AAGCAGTGGTATCAACGCAGAGTGAATrGrGrG-3′), 8.33 mM dithiothreitol (Bioworld, 40420001-1), 1.67 M Betaine (Sigma, B0300-5VL) and 10 mM $MgCl_2$ (Sigma, M1028-10X1ML)], was added with a Formulatrix Mantis liquid handler. The reaction was then carried out by incubating wells on a thermocycler (Bio-Rad) at 42 °C for 90 min, and stopped by heating at 70 °C for 5 min. Subsequently, 3.75 units of PCR mix (1.67× KAPA HiFi HotStart ReadyMix (Kapa Biosystems, KK2602), 0.17 µM IS PCR primer (IDT, 5′-AAGCAGTGGTAT CAACGCAGAGT-3′), and 0.038 U/µL Lambda Exonuclease (NEB, M0262L) was added to each well. PCR was then performed using the following program: 1) 37 °C for 30 min, 2) 95 °C for 3 min, 3) 21 cycles of 98 °C for 20 s, 67 °C for 15 s and 72 °C for 4 min, and 4) 72 °C for 5 min. cDNA from every well was quantified using Quant-iT™ PicoGreen™ dsDNA Assay Kit (Thermo Fisher: P11496), and diluted to 0.4 ng/µL in Tris-EDTA before tagmentation. Before tagmentation, we reformatted the samples into a standardized 384-well format, and used the Formulatrix Mantis and Mosquito (TTP Labtech) to automatically perform all liquid handling steps. Tagmentation was performed on double-stranded cDNA using the Nextera XT Library Sample Preparation kit (Illumina, FC-131-1096). Each well was mixed with 0.8 µL Nextera tagmentation DNA buffer and 0.4 µL Tn5 enzyme, then incubated at 55 °C for 10 min. The reaction was stopped by adding 0.4 µL Neutralization Buffer and centrifuging at room temperature at 3,220 *g* for 5 min. Indexing PCR reactions were performed by adding 0.4 µL of 5 µM i5 indexing primer, 0.4 µl of 5 µM i7 indexing primer, and 1.2 µL of Nextera NPM mix. PCR amplification was carried out using the following program: 1) 72 °C for 3 min, 2) 95 °C for 30 s, 3) 12 cycles of 95 °C for 10 s, 55 °C for 30 s and 72 °C for 1 min, and 4) 72 °C for 5 min. After library

preparation, wells of each 384-library plate were pooled using a Mosquito liquid handler, and consolidated into one tube. Pooling was followed by two final purifications using 0.8× AMPure beads (Fisher, A63881). Library quality was assessed using capillary electrophoresis on a Fragment Analyzer (AATI), and libraries were quantified by qPCR (Kapa Biosystems, KK4923) on a CFX96 Touch Real-Time PCR Detection System (Bio-Rad). Libraries were sequenced on the NovaSeq 6000 Sequencing Systems (Illumina) using 2 × 100-bp paired-end reads, respectively. Sequences were de-multiplexed using bcl2fastq. Reads were aligned to the mouse mm10 genome (with Cre and tdTomato genes added) using STAR version 2.5.4[53]. Gene counts were produced using HTseq version 0.10.0[54], for only exons, with the 'intersection-strict' flag. The raw data resulting from this was a matrix 4045 cells × 21171 genes.

Single-cell sequencing data analysis. Before generating the transcriptomic map featured in **Extended Data Fig. 1b**, we first coarsely analyzed the cell datasets from each dissected region individually (pCA1, dCA1, pSub, dSub, MEC, LEC) to identify cells that should be: 1) removed from the dataset based on the expression of known markers from unrelated contaminating regions such as CA2/3), or 2) unambiguously relabeled as a different region based on marker expression. To do this, we first removed cells if they expressed fewer than 2000 genes, and removed genes if they were detected in fewer than 3 cells. This resulted in a dataset of 3691 cells × 18865 genes. We aimed for our dataset to contain > 500 cells for each subregion, and collected cells in batches until this number was reached. The breakdown of the 3691 cell dataset was pCA1: 701 cells, 3 batches; dCA1: 780 cells, 2 batches; pSub: 500 cells, 1 batch; dSub: 678 cells, 1 batch; MEC: 507 cells, 1 batch; LEC: 525 cells, 1 batch. We next subsetted this data based on the 6 dissection regions, and used default settings for filtering, variable gene selection, dimensionality reduction, and clustering (resolution = 0.5) in Seurat v3.0[55]. This resulted in a Seurat object for each dissected region, where cells were visualized using a 2-dimensional t-distributed stochastic neighbor embedding (tSNE) of the PC-projected data, and differential expression marker analysis could be performed to identify cell clusters that should be removed or re-labeled. This resulted in between 5 and 10 clusters for each subregion dataset (**Extended Data Fig. 2**). To identify marker genes for the clusters in each subregion, we used the FindAllMarkers function in Seurat v3.0 and applied this to each Seurat object. This function performs differential expression analysis (Wilcoxon rank sum) between a specific cluster, compared with all other cells not in the cluster, and then iterates through all clusters. Within Seurat, "PCT" refers to the fraction of cells within a population expressing a specific gene. We considered only marker genes that were expressed in at least 25% of cells in either of the comparison groups (min.pct = 0.25), and exhibited a log fold change threshold > 0.25, and plotted the top 10 genes for each cluster using the DoHeatmap function (**Extended Data Fig. 2**) for visualization. To characterize the anatomical identity of each cluster, we checked the expression pattern of the top 10 genes using *in situ* hybridization images from Allen Institute website (www.mouse.brain-map.org)[50]. Those clusters which were enriched for genes not in CA1, subiculum or entorhinal cortex were removed (i.e., CA2/3 and presubiculum). Those clusters which were enriched for genes not from their dissected region but still from CA1, subiculum, or entorhinal were re-classified (i.e., dCA1 cells re-classified as pSub).

Generation of the transcriptomic map in Extended Data Fig. 1b. Following the removal of contaminating cells and the relabeling of cells based on region, we generated the final Seurat object

featured in **Extended Data Fig. 1b** under the following conditions. As before, cells expressing fewer than 2000 genes and genes detected in fewer than 3 cells were already removed. We also removed cells expressing *Gad2* > 0, as these were putative inhibitory neurons. This resulted in a final, high-quality dataset of 3382 cells × 18724 genes, where the median cell expressed 6254 genes, from 759819 reads. Cell counts based on the re-labeled regions were: pCA1: 582, dCA1: 682, pSub: 582, dSub 509, MEC: 505, LEC: 522. To generate the tSNE map in **Extended Data Fig. 1b** , a Seurat object was generated similar to before with default settings. Of note, we performed the ScaleData function and regressed out the effects of the # of genes and the # of reads, and 11 PCs were used in the FindNeighbors function based on a steep dropoff in variance explained by visual inspection of the elbow plot. Cells were visualized using the DimPlot, FeaturePlot, and VlnPlot functions.

Identification of genes with inverse expression to Ten3. To identify genes with inverse expression to Ten3 across CA1, subiculum, and entorhinal cortex, we first subsetted the total data into three groups based on the updated region labels. Within each region, we next identified cells with expression of Ten3 (*Odz3)* in the top 95th percentile in each region, and labeled these as *Ten3*-HIGH. Conversely, we identified the cells with no expression of Ten3 in each region, and labeled these as *Ten3*-NONE. Thus, for each region (CA1, Sub, EC) we had a set of *Ten3*-HIGH and *Ten3*-NONE cells to compare gene expression. To perform differential expression, we compared *Ten3*-HIGH and *Ten3*-NONE cells in each region using the FindMarkers function in Seurat v3.0, which uses the Wilcoxon rank sum test. Compared to our coarse survey of region-based marker genes, we more stringently considered only genes that were expressed in at least 50% of cells in either of the comparison groups (min.pct = 0.5). We also required that the difference in membership between the two groups ($PCT_{Ten3\text{-HIGH}} - PCT_{Ten3\text{-NONE}}$) for considered genes to be >0.1 (min.diff.pct = 0.1). We next took all genes that exhibited higher average expression in the *Ten3*-NONE groups for each of the regions, and computed the intersection of these to arrive at the list of 11 genes in **Fig. 1b**.

Double *in situ* hybridization. Mice were injected with 2.5% Avertin and were transcardially perfused with PBS followed by 4% paraformaldehyde (PFA). Brains were dissected and post-fixed in 4% PFA for 1 hour, cryoprotected for about 24 hours in 30% sucrose. Brains were embedded in Optimum Cutting Temperature (OCT, Tissue-Tek), frozen in dry ice cooled isopentane bath and stored at –80°C until sectioned. *In situ* hybridizations were performed as previously described[56] with the following modifications. 16-µm sections were collected on Superfrost Plus slides and used for fluorescent *in situ* hybridization. *Ten3* and *Lphn2* probes were amplified using primer pairs F-5'-GTGGCTAAAAGCCCACTGTTGCC-3', R-5'-GAATGGCCCACTGACCTCGCG-3' and F-5'-ACCAGTAGCAATCAAGCCACA -3', R-5'-AAGGACCACCTTGGTCGAGT-3', respectively. PCR products were cloned into *pCR4-TOPO* (K457502) and RNA probes were transcribed using T3 or T7 RNA polymerases. *Ten3* probe was labeled with fluorescein (Roche 11685619910) and *Lphn2* probe was labeled with DIG (Roche 11277073910). Slides were hybridized, washed, blocked and incubated with alkaline phosphatase-conjugated anti-DIG-AP antibody (1:1,000, Roche 11093274910) and anti-Fluorescein-HRP (1:200, Perkin Elmer NEF710001EA). Sections were developed with TSA-Plus Fluoroscein system (NEL741001KT) for 15 minutes, 3 hrs with Fast Red TR/Naphthol As-MX (Sigma

F4523), counterstained with DAPI, washed and mounted with Fluoromount-G (SouthernBiotech). Sections were imaged using the tile scan function on Zeiss LSM 780 confocal microscope (10x magnification). Fluorescence intensity measurements on unprocessed images were taken using FIJI and data processing was performed using MATLAB. For CA1 measurements, a 75-pixel-wide segmented line was drawn along the cell body layer from proximal to distal. pCA1 was determined by increased DAPI intensity versus CA2 and dCA1 was determined by the condensed CA1 cell body layer disappearing. For subiculum quantification, a 200-pixel-wide segmented line was drawn through the cell body layer from proximal to distal. pSub was defined by the region adjacent to the CA1 cell body layer and dSub was defined as the regions directly before the cell dense presubiculum. For entorhinal cortex, a 250-pixel-wide segmented line was drawn from medial to lateral. Segmented lines were drawn, straightened using the Straighten function, background subtraction was performed using the Subtract function and intensity values were measured using the Plot Profile command (performed in FIJI). The intensity plots were resampled into 100 equal bins (MATLAB) and each individual trace was normalized to a maximum of 100. Traces from each animal were averaged, normalized to a maximum of 100 again and then the normalized average trace from each animal was combined to give the final distribution (**Fig. 1** and **Extended Data Fig. 3**). Numbers of sections used for quantifications are as follows: horizontal section CA1: 10, 9, 10 sections from 3 mice; horizontal section subiculum: 10, 10, 11 sections from 3 mice; horizontal section entorhinal cortex: 5, 9, 8 sections from 3 mice; sagittal section CA1: 8, 8, 4 sections from 3 mice; and sagittal section subiculum: 8, 7, 4 sections from 3 mice.

Immunostaining. Mice were injected with 2.5% Avertin and were transcardially perfused with PBS followed by 4% paraformaldehyde (PFA). Brains were dissected and post-fixed in 4% PFA for 1 hour (for P8 Ten3 and Lphn2 staining) or 4–6 hours (for adult GFP and mCh staining), cryoprotected for about 24 hours in 30% sucrose. Brains were embedded in Optimum Cutting Temperature (OCT, Tissue-Tek), frozen in dry ice cooled isopentane bath and stored at –80°C until sectioned. 60-µm thick floating sections were collected in PBS + 0.02% sodium azide and stored at 4°C. Sections were incubated in the following solutions at room temperature unless indicated: 1 hour in 0.3% PBS/Triton X-100 and 10% normal donkey serum, two nights (adult GFP and mCh staining) or four nights (P8 Ten3 and Lphn2 staining) in primary antibody at 4°C in 0.3% PBS/Triton X-100 and 10% normal donkey serum, 3 × 15 min in 0.3% PBS/Triton X-100, overnight in secondary antibody + DAPI (1:10,000 of 5 mg ml^{-1}, Sigma-Aldrich) in 0.3% PBS/Triton X-100 and 10% normal donkey serum, 2 × 15 min in 0.3% PBS/Triton X-100, and 15 min in PBS. Sections were mounted with Fluoromount-G (SouthernBiotech). Primary antibodies used were rabbit anti Ten3 (1:500)[5], chicken anti-GFP (1:2,500, Aves Labs, GFP-1020) and rat anti-mCherry (1:1,000, Thermo Fisher, M11217). Secondary antibodies conjugated to Alexa 488, Alexa 568, or Cy3 (Jackson ImmunoResearch) were used at 1:500 from 50% glycerol stocks. For quantification of Lphn2 and Ten3 protein images were taken with a Zeiss LSM 780 confocal microscope (10x magnification) and quantification was done as described for *in situ* hybridization except fluorescence intensity measurements were taken from the molecular layers of CA1 (150 pixels wide) and subiculum (150 pixels wide) and layer III of the entorhinal cortex (250 pixels wide). Numbers of sections used for quantifications are as follows: horizontal CA1: 10, 7, 6 sections from 3 mice; horizontal subiculum: 11, 7, 4 sections from 3 mice; horizontal entorhinal cortex: 5, 4, 5 sections from 3 mice; sagittal CA1: 10, 10 sections from 2 mice; and

sagittal subiculum: 10, 10 sections from 2 mice. Sections for pCA1 axon quantification in subiculum were imaged using a Zeiss epifluorescence microscope.

Aggregation assay. K562 cells (ATCC, CCL-243) were grown in RPMI-1640 + Glutamax (Gibco, 61870127) with 10% FBS (Gibco A3160501) and 1× penicillin/streptomycin (Gibco 15140122). K562 cells were electroporated with Neon Transfection System 100-µl tips (Thermo Fisher MPK5000) using 1450 V, 10 ms, and 3 pulses. The following amounts of dual reporter plasmid (gene of interest and fluorescent reporter in the same construct) were used: 15 µg of *Ef1α-Ten3 CMV–GFP*, 10.9 µg of *Ef1α-Lphn2*;*CMV–mCh*, 5µg *Ef1α- Empty*;*CMV–mCh* and 5µg *Ef1α- Empty;CMV–GFP*. For each electroporation, 2 ×10^6 cells were washed in PBS, resuspended in 120 µl of buffer R, combined with DNA and electroporated. Cells were added to 5 ml of pre-warmed RPMI-1640 with 10% FBS and incubated at 37°C and 5%CO_2 for ~20 hours. Cells were collected and resuspended in RPMI-1640 + 10% FBS and incubated for 15 min at 37 °C with 0.1 mg/ml DNase (Worthington LS002060). Cells were resuspended in aggregation media (Neurobasal-A, 4% B27, 2 mM glutamine, 10% FBS, 20 mM HEPES) and passed through a 40µm cell strainer. 2 ×10^5 cells of each condition (4 ×10^5 total) were added to wells of a 24-well plate in 1 ml of aggregation media and cells were left to aggregate for 1–2 hours on a nutator at 37°C. Cells were transferred to 2 ml of PBS in a 6-well plate and aggregates were imaged with a Nikon Eclipse Ti microscope at 4× magnification. *Ef1α-Ten3 CMV–GFP*, *Ef1α- Empty CMV–mCh* and *Ef1α- Empty CMV–GFP* were previously generated[5] and *Ef1α-Lphn2 CMV–mCh* was generated by using Gibson assembly cloning kit (NEB E5510S) to insert *Lphn2* ORF into *Ef1α- Empty CMV–mCh*. Full length *Lphn2* was amplified from cDNA isolated from P8 mouse hippocampus. The *Ten3* isoform used contained both NHL and EGF domain alternatively spliced exons (the A_1B_1 isoform[5]), which is the highest expressed isoform during the development of the CA1→Sub axon projection[5].

Lentivirus production. *LV-UbC-GFP-Cre* was generated by the Neuroscience Gene Vector and Virus core, Stanford University. All other lentivirus constructs were made by inserting either *GFP*, *Lphn2* or *Lphn2_ΔLEC* into the *LV-UbC* plasmid with a P2A sequence between the two ORFs. *GFP* was amplified from *LV-UbC-GFP-Cre* and full length *Lphn2* was isolated from P8 mouse hippocampus cDNA. *GFP* and *Lphn2* were inserted into *LV-UbC* with Gibson assembly cloning kit (NEB E5510S) and the *Lphn2_ΔLEC* mutation was made using Q5 mutagenesis (NEB, E0552S). All plasmids were sequenced verified before virus was produced. All custom lentiviruses were generated by transfecting 30 10-cm plates (HEK293T) with 4 plasmids (4.1R, RTR2, VSVg, and transfer vector containing gene of interests). Medium was collected 48 hrs later and centrifuge at 7000 rcf for 18 hrs at 4°C. Viral pellets were dissolved with PBS and further purified with a HiPrep Q FF (16/10) ion-exchange column (GE healthcare)[57]. The final concentration of individual lentivirus ranged from 1 × 10^{11} to 6 × 10^{12} infectious copies per ml.

Stereotactic injections in neonatal mice. P0 mice were anesthetized using hypothermia. Subiculum injections were 1.1–1.2 mm lateral, 0.3–0.35 mm anterior and 0.85 mm ventral from lambda. 100 nl of lentivirus was injected at 100 nl min^{-1} at the following titers: *LV-UbC-GFP* (6 × 10^{12} infectious copies per ml), *LV-UbC-GFP-P2A-Lphn2-FLAG* (6 × 10^{11}–5 × 10^{12} infectious copies per ml), *LV-UbC-GFP-P2A-Lphn2_ΔLEC-FLAG* (1 × 10^{11}–4 ×10^{11} infectious copies per ml), *LV-UbC-GFP-Cre* (1.3 × 10^8–5.9

$\times 10^8$ infectious copies per ml, Neuroscience Gene Vector and Virus core, Stanford University). 200 nl was injected into *Lphn2*$^{fl/fl}$*;Ten3*$^{fl/fl}$ mice (**Fig. 4**).

Stereotactic injections in adult mice. Injections of *AAV8-CaMKIIa-ChR2-mCh* (2×10^{12} infectious copies per ml, Neuroscience Gene Vector and Virus core, Stanford University) and *AAV8- CaMKIIa-ChR2-YFP* (2×10^{12} infectious copies per ml, Neuroscience Gene Vector and Virus core, Stanford University) were performed at about P36. Mice were anesthetized using isoflurane and mounted in stereotactic apparatus (Kopf). Coordinates for pCA1 were 1.4 mm lateral and 0.9–1.25 mm posterior from bregma, and 1.0–1.12 mm ventral from brain surface; dSub were 3.4 mm lateral, 0 mm anterior, 2.0 mm ventral; msub were 3.6 mm lateral, 0.2 mm anterior, 2.0 mm ventral. Virus was iontophoretically injected with current parameters 5 µA, 7 s on, 7 s off, for 2 min, using pipette tips with an outside perimeter of 10–15 µm. Mice were perfused about 2 weeks later and processed for immunostaining as described above.

Image and data analysis for CA1 axon tracing. Mice were only included if they passed the following criteria: (1) AAV injection site must be in pCA1 (most proximal 30%) – based on *Ten3* mRNA in sagittal sections (**Extended Data Fig. 10**); (2) lentivirus injections must be in the subiculum, more specifically in dSub for experiments described in **Fig. 2**, in mSub and/or pSub for experiments described in **Fig. 3**, and in both dSub and pSub for experiments described in **Fig. 4**; and (3) pCA1 axons must overlap with lentivirus injection site in subiculum. All mice that fulfilled these criteria are reported in **Figs. 2–4** and **Extended Data Figs. 6–8**, and were included in quantifications. Images of injections sites (5× magnification) and projections (10× magnification) were acquired of every other 60-µm sagittal section using a Zeiss epifluorescence scope. Due to variation in injection sites within each animal, exposure was adjusted for each animal to avoid saturation. Fluorescence intensity measurements on unprocessed images were taken using FIJI and data processing was performed using MATLAB. For injection site quantification, a 30-pixel-wide segmented line was drawn from pCA1 to dCA1 using DAPI signal as a guide. For projection quantification in subiculum, a 200-pixel-wide segmented line was drawn from pSub to dSub through the cell body layer using only DAPI as a guide. From this point injection site and projection images were processed the same. Segmented lines were straightened using the Straighten function, background subtraction was performed using the Subtract function and intensity values were measured using the Plot Profile command (FIJI). For injections that labeled both CA2 and pCA1, CA2 axons were present near the distal border of CA1 and spilled into pSub. These axons had their intensity set to zero by using area selection and the clear function (FIJI). The intensity plots were resampled into 100 equal bins using a custom MATLAB code. Heatmaps were generated in MATLAB using the 'imagesc' function and three-dimensional mountain plots were generated using the 'surf' function. For trace quantification in **Fig. 3** and **Fig. 4**, only sections with GFP-Cre expression in the correct subiculum area were quantified. Each individual trace was normalized to a maximum of 100, traces from each animal were averaged, normalized to a maximum of 100 again and then the normalized average traces for each animal within a condition were combined. The mean position of the trace (injection or projection) was calculated by multiplying the intensity value by the bin position, summing across the entire axis, and dividing by the sum of the intensity values. The projection width was calculated using the MATLAB script 'width=fwhm(x,y)'. The peak of the traces was determined by using the GraphPad Prism 'area under curve

– peak x' value. All statistical comparisons were performed using an unpaired two-tailed t-test in GraphPad Prism 7. Representative images (**Extended Data Fig. 6–8**) were taken using a Zeiss LSM 780 confocal microscope (20× magnification, tile scan, max projection) and all images from each individual animal were processed identically.

Code availability. Custom MATLAB scripts used in data processing and analysis are available from the corresponding author upon reasonable request.

Data availability. All data supporting the findings reported in this study are available from the corresponding author upon reasonable request. The single-cell RNA-seq datasets generated and analyzed in the study will be deposited in NCBI Gene Expression Omnibus.

References

1. Igarashi, K. M., Ito, H. T., Moser, E. I. & Moser, M.-B. Functional diversity along the transverse axis of hippocampal area CA1. *FEBS Lett.* **588**, 2470–2476 (2014).
2. Cembrowski, M. S. *et al.* Dissociable Structural and Functional Hippocampal Outputs via Distinct Subiculum Cell Classes. *Cell* **173**, 1280-1292.e18 (2018).
3. Naber, P. A., Lopes da Silva, F. H. & Witter, M. P. Reciprocal connections between the entorhinal cortex and hippocampal fields CA1 and the subiculum are in register with the projections from CA1 to the subiculum. *Hippocampus* **11**, 99–104 (2001).
4. Tamamaki, N. & Nojyo, Y. Preservation of topography in the connections between the subiculum, field CA1, and the entorhinal cortex in rats. *J. Comp. Neurol.* **353**, 379–390 (1995).
5. Berns, D. S., DeNardo, L. A., Pederick, D. T. & Luo, L. Teneurin-3 controls topographic circuit assembly in the hippocampus. *Nature* **554**, 328–333 (2018).
6. Silva, J.-P. *et al.* Latrophilin 1 and its endogenous ligand Lasso/teneurin-2 form a high-affinity transsynaptic receptor pair with signaling capabilities. *Proc. Natl. Acad. Sci. U. S. A.* **108**, 12113–12118 (2011).
7. Boucard, A. A., Maxeiner, S. & Südhof, T. C. Latrophilins function as heterophilic cell-adhesion molecules by binding to teneurins: regulation by alternative splicing. *J. Biol. Chem.* **289**, 387–402 (2014).
8. O'Sullivan, M. L. *et al.* FLRT proteins are endogenous latrophilin ligands and regulate excitatory synapse development. *Neuron* **73**, 903–910 (2012).
9. Sanes, J. R. & Yamagata, M. Many Paths to Synaptic Specificity. *Annu. Rev. Cell Dev. Biol.* **25**, 161–195 (2009).
10. Yogev, S. & Shen, K. Cellular and molecular mechanisms of synaptic specificity. *Annu. Rev. Cell Dev. Biol.* **30**, 417–437 (2014).

11. Kolodkin, A. L. & Tessier-Lavigne, M. Mechanisms and molecules of neuronal wiring: a primer. *Cold Spring Harb. Perspect. Biol.* **3**, (2011).

12. Südhof, T. C. Towards an Understanding of Synapse Formation. *Neuron* **100**, 276–293 (2018).

13. Sperry, R. W. Chemoaffinity in the Orderly Growth of Nerve Fiber Patterns and Connections. *Proc. Natl. Acad. Sci.* **50**, 703–710 (1963).

14. Hong, W., Mosca, T. J. & Luo, L. Teneurins instruct synaptic partner matching in an olfactory map. *Nature* **484**, 201–207 (2012).

15. Mosca, T. J., Hong, W., Dani, V. S., Favaloro, V. & Luo, L. Trans-synaptic Teneurin signalling in neuromuscular synapse organization and target choice. *Nature* **484**, 237–241 (2012).

16. Li, H., Bishop, K. M. & O'Leary, D. D. M. Potential target genes of EMX2 include Odz/Ten-M and other gene families with implications for cortical patterning. *Mol. Cell. Neurosci.* **33**, 136–149 (2006).

17. del Toro, D. *et al.* Structural Basis of Teneurin-Latrophilin Interaction in Repulsive Guidance of Migrating Neurons. *Cell* **180**, 323-339.e19 (2020).

18. Leamey, C. A. *et al.* Ten_m3 regulates eye-specific patterning in the mammalian visual pathway and is required for binocular vision. *PLoS Biol.* **5**, e241 (2007).

19. Dharmaratne, N. *et al.* Ten-m3 Is Required for the Development of Topography in the Ipsilateral Retinocollicular Pathway. *PLoS ONE* **7**, (2012).

20. Antinucci, P., Nikolaou, N., Meyer, M. P. & Hindges, R. Teneurin-3 Specifies Morphological and Functional Connectivity of Retinal Ganglion Cells in the Vertebrate Visual System. *Cell Rep.* **5**, 582–592 (2013).

21. Antinucci, P., Suleyman, O., Monfries, C. & Hindges, R. Neural Mechanisms Generating Orientation Selectivity in the Retina. *Curr. Biol.* **26**, 1802–1815 (2016).

22. Sando, R., Jiang, X. & Südhof, T. C. Latrophilin GPCRs direct synapse specificity by coincident binding of FLRTs and teneurins. *Science* **363**, (2019).

23. Croarkin, P. E. *et al.* Genetic Risk Score Analysis in Early-Onset Bipolar Disorder. *J. Clin. Psychiatry* **78**, 1337–1343 (2017).

24. Green, E. K. *et al.* Replication of bipolar disorder susceptibility alleles and identification of two novel genome-wide significant associations in a new bipolar disorder case-control sample. *Mol. Psychiatry* **18**, 1302–1307 (2013).

25. Mühleisen, T. W. *et al.* Genome-wide association study reveals two new risk loci for bipolar disorder. *Nat. Commun.* **5**, 3339 (2014).

26. Ivorra, J. L. *et al.* Replication of previous genome-wide association studies of psychiatric diseases in a large schizophrenia case-control sample from Spain. *Schizophr. Res.* **159**, 107–113 (2014).

27. Aldahmesh, M. A., Mohammed, J. Y., Al-Hazzaa, S. & Alkuraya, F. S. Homozygous null mutation in ODZ3 causes microphthalmia in humans. *Genet. Med. Off. J. Am. Coll. Med. Genet.* **14**, 900–904 (2012).

28. Alkelai, A. *et al.* A role for TENM1 mutations in congenital general anosmia. *Clin. Genet.* **90**, 211–219 (2016).

29. Li, J. *et al.* Structural Basis for Teneurin Function in Circuit-Wiring: A Toxin Motif at the Synapse. *Cell* **173**, 735-748.e15 (2018).

30. Vysokov, N. V. *et al.* Proteolytically released Lasso/teneurin-2 induces axonal attraction by interacting with latrophilin-1 on axonal growth cones. *eLife* **7**, e37935 (2018).

31. Anderson, G. R. *et al.* Postsynaptic adhesion GPCR latrophilin-2 mediates target recognition in entorhinal-hippocampal synapse assembly. *J Cell Biol* jcb.201703042 (2017) doi:10.1083/jcb.201703042.

32. Witter, M. P. & Groenewegen, H. J. The subiculum: cytoarchitectonically a simple structure, but hodologically complex. *Prog. Brain Res.* **83**, 47–58 (1990).

33. Wright, N. F., Vann, S. D., Erichsen, J. T., O'Mara, S. M. & Aggleton, J. P. Segregation of parallel inputs to the anteromedial and anteroventral thalamic nuclei of the rat. *J. Comp. Neurol.* **521**, 2966–2986 (2013).

34. Meibach, R. C. & Siegel, A. Efferent connections of the septal area in the rat: an analysis utilizing retrograde and anterograde transport methods. *Brain Res.* **119**, 1–20 (1977).

35. Ishizuka, N. Laminar organization of the pyramidal cell layer of the subiculum in the rat. *J. Comp. Neurol.* **435**, 89–110 (2001).

36. Wright, N. F., Erichsen, J. T., Vann, S. D., O'Mara, S. M. & Aggleton, J. P. Parallel but separate inputs from limbic cortices to the mammillary bodies and anterior thalamic nuclei in the rat. *J. Comp. Neurol.* **518**, 2334–2354 (2010).

37. Araç, D. *et al.* A novel evolutionarily conserved domain of cell-adhesion GPCRs mediates autoproteolysis. *EMBO J.* **31**, 1364–1378 (2012).

38. Zimmer, M., Palmer, A., Köhler, J. & Klein, R. EphB-ephrinB bi-directional endocytosis terminates adhesion allowing contact mediated repulsion. *Nat. Cell Biol.* **5**, 869–878 (2003).

39. Hattori, M., Osterfield, M. & Flanagan, J. G. Regulated cleavage of a contact-mediated axon repellent. *Science* **289**, 1360–1365 (2000).

40. Popova, N. V., Deyev, I. E. & Petrenko, A. G. Association of adaptor protein TRIP8b with clathrin. *J. Neurochem.* **118**, 988–998 (2011).

41. Popova, N. V., Plotnikov, A., Deev, I. E. & Petrenko, A. G. Interaction of calcium-independent latrotoxin receptor with intracellular adapter protein TRIP8b. *Dokl. Biochem. Biophys.* **414**, 149–151 (2007).

42. Yamagishi, S. *et al.* FLRT2 and FLRT3 act as repulsive guidance cues for Unc5-positive neurons. *EMBO J.* **30**, 2920–2933 (2011).

43. Jackson, V. A. *et al.* Structural Basis of Latrophilin-FLRT Interaction. *Struct. England1993* **23**, 774–781 (2015).

44. Seiradake, E. *et al.* FLRT Structure: Balancing Repulsion and Cell Adhesion in Cortical and Vascular Development. *Neuron* **84**, 370–385 (2014).

45. Brose, K. *et al.* Slit proteins bind Robo receptors and have an evolutionarily conserved role in repulsive axon guidance. *Cell* **96**, 795–806 (1999).

46. Wu, Z. *et al.* Long-Range Guidance of Spinal Commissural Axons by Netrin1 and Sonic Hedgehog from Midline Floor Plate Cells. *Neuron* **101**, 635-647.e4 (2019).

47. Matsuoka, R. L. *et al.* Transmembrane semaphorin signaling controls laminar stratification in the mammalian retina. *Nature* **470**, 259–263 (2011).

48. Duan, X. *et al.* Cadherin Combinations Recruit Dendrites of Distinct Retinal Neurons to a Shared Interneuronal Scaffold. *Neuron* **99**, 1145-1154.e6 (2018).

49. Picelli, S. *et al.* Full-length RNA-seq from single cells using Smart-seq2. *Nat. Protoc.* **9**, 171–181 (2014).

50. Lein, E. S. *et al.* Genome-wide atlas of gene expression in the adult mouse brain. *Nature* **445**, 168–176 (2007).

51. Harris, J. A. *et al.* Anatomical characterization of Cre driver mice for neural circuit mapping and manipulation. *Front. Neural Circuits* **8**, 76 (2014).

52. Madisen, L. *et al.* A robust and high-throughput Cre reporting and characterization system for the whole mouse brain. *Nat. Neurosci.* **13**, 133–140 (2010).

53. Dobin, A. *et al.* STAR: ultrafast universal RNA-seq aligner. *Bioinformatics* **29**, 15–21 (2013).

54. Anders, S., Pyl, P. T. & Huber, W. HTSeq--a Python framework to work with high-throughput sequencing data. *Bioinforma. Oxf. Engl.* **31**, 166–169 (2015).

55. Butler, A., Hoffman, P., Smibert, P., Papalexi, E. & Satija, R. Integrating single-cell transcriptomic data across different conditions, technologies, and species. *Nat. Biotechnol.* **36**, 411–420 (2018).

56. Weissbourd, B. *et al.* Presynaptic partners of dorsal raphe serotonergic and GABAergic neurons. *Neuron* **83**, 645–662 (2014).

57. Kinoshita, M. *et al.* Genetic dissection of the circuit for hand dexterity in primates. *Nature* **487**, 235–238 (2012).

Acknowledgements We thank T. Südhof for the *Lphn2*^{mVenus} and *Lphn2*^{fl} mice, the Neuroscience Gene Vector and Virus Core at Stanford University for producing viruses, D. Berns for advice, inspiration, and artwork (Fig. 1a, j), J. Ferguson for artwork (Fig. 2a and Fig. 5g), M. Wagner and J. Kebschull for custom MATLAB code, members of the Luo lab for advice and support, D. Berns, J. Kebschull, A. Khalaj, H. Li, J. Li, T. Li, C. McLaughlin, K. Shen and A. Shuster for critiques of the manuscript. D.T.P. was supported by an American Australian Association Education Fund Scholarship. L.L. is an investigator of Howard Hughes Medical Institute. This work was supported by National Institutes of Health grant (R01-NS050580 to L.L.)

Author Contributions D.T.P. performed all the experiments and analyzed the data, except for single-cell sequencing sample collection and data processing which was performed by J.H.L., with support from S.R.Q. E.C.G. and C.X. assisted in tissue processing. Y.L. and Z.H. produced custom lentivirus. L.L. supervised the study. D.T.P., J.H.L., and L.L. wrote the paper.